Stimulated Recovery of Radiation Damage in cooled PbWO$_4$-Crystals for the $\overline{\text{P}}$ANDA Detector

Diplomarbeit
im Fachgebiet Experimentalphysik
Prof. Dr. Volker Metag
II. Physikalisches Institut
Universität Gießen

vorgelegt von

Till Kuske
aus Bad Nauheim

Betreuer: Dr. Rainer Novotny

for my sister

Antje

1979 - 2003

... thank you for the smile upon your face.
... thank you, thank you for the gleam that shows its grace

Contents

Contents

Summary

To achieve the physics goals of the $\overline{P}$ANDA-detector lead tungstate has been chosen as the scintillator for the electromagnetic calorimeter. The scintillator is required to deliver high performance and stability in a hazardous high radiation environment. Every scintillation material under this condition is subject to radiation damage, in the case of PWO mostly in the formation of color centers with wide absorption bands leading. This transmission loss directly affects the detector performance. A new regeneration method, stimulated recovery by illumination, was discovered to achieve impressive results at room temperature. The goal of this thesis was to determine if stimulated recovery can be applied at T=$-25°C$, the operating temperature of the $\overline{P}$ANDA-EMC. As demonstrated by the results this is possible. The main differences between stimulated recovery at low temperature compared to room temperature manifests in longer timescales and no full recovery. It is also photon flux dependent up to a given limit for specific dose rates and shows an equilibrium. Furthermore it is shown that stimulated recovery does not work for wavelengths above ≈940nm as opposed to the room temperature data. EPR studies were conducted to find the color centers and traps, which respond to this recovery method. This showed a metastable formation of $(MoO_4)^{3-}$-traps which retrap the released electrons of annihilated deep centers. This is in good accord with the signal response measurements for stimulated recovery, as this trap does not impact the main luminescence. The cutoff at ≈940nm gives an indication of the depth of the affected trap. It hints toward a 700meV deep Frenkel type defect in the WO_4 structure. Finally a study of online recovery was conducted, the in situ illumination with light while irradiating the crystals. From the data it can be deduced that online recovery is feasible for short wavelengths. For low dose rates this can improve the stable long term operation of PWO scintillators.

Chapter 1

Introduction

To perform strong interaction studies by observing the annihilation of antiprotons and initiated reactions the $\overline{\mathrm{P}}$ANDA[1] experiment will be build at the future FAIR[2] facility at GSI[3] in Darmstadt. The $\overline{\mathrm{P}}$ANDA detector is located at the new HESR[4] which will store and accelerate the antiproton beam.
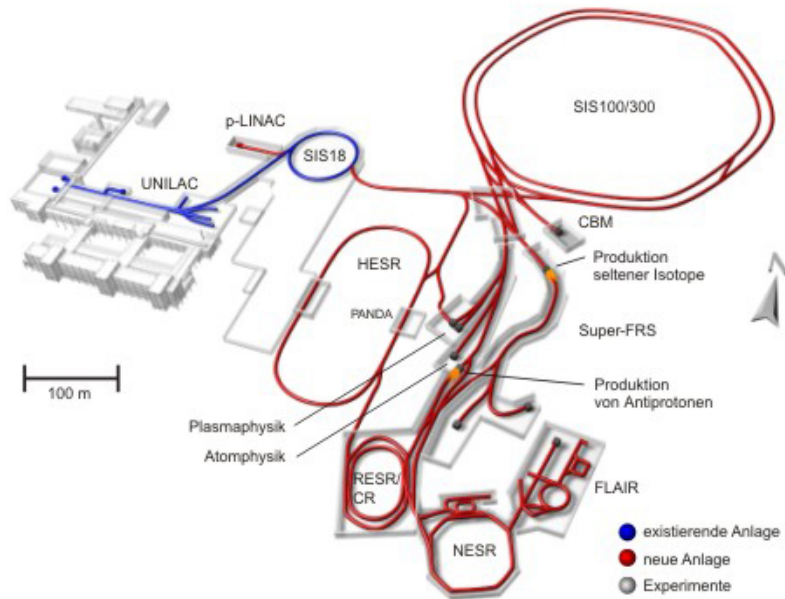

Figure 1.1: Present GSI with the planned FAIR facility [Met08].

The accelerator facility will make use of the existing SIS18 as injector for the new SIS100/300. This two stage synchrotron concept provides high intensities of heavy ion

---

[1]$\overline{\mathrm{P}}$ANDA = anti$\underline{\mathrm{P}}$roton $\underline{\mathrm{AN}}$nihilation at $\underline{\mathrm{DA}}$rmstadt
[2]FAIR = $\underline{\mathrm{F}}$acility for $\underline{\mathrm{A}}$ntiproton and $\underline{\mathrm{I}}$on $\underline{\mathrm{R}}$esearch
[3]GSI = $\underline{\mathrm{G}}$esellschaft für $\underline{\mathrm{S}}$chwer$\underline{\mathrm{I}}$onenforschung
[4]HESR = $\underline{\mathrm{H}}$igh $\underline{\mathrm{E}}$nergy $\underline{\mathrm{St}}$orage $\underline{\mathrm{R}}$ing

and proton beams which allow the efficient production of secondary beams consisting of exotic atomic nuclei or antiprotons. These secondary beams can be collected in different storage rings. One of them is the HESR, by usage of stochastical and electron cooling, capable providing an antiproton beam in a broad momentum range between $1.5 \frac{\text{GeV}}{\text{c}}$ to $15 \frac{\text{GeV}}{\text{c}}$ with a maximum luminosity of $2 \cdot 10^{32} \frac{1}{\text{cm}^2\text{s}}$. The cooling concept allow either a high liminosity with moderate momentum resolution for studies with low crosssection or high resolution at moderate intesity for precision measurements. The scientific program of $\overline{\text{P}}$ANDA includes several aspects, mostly in the non-perturbative regime, listed below [Col09, Met08]:

- Charmonium spectroscopy

- Searching for exotic states like glueballs, hybrids and multiquark states

- Open charm spectroscopy

- Investigation of hadron properties inside nuclear matter

- Hypernuclear physics

- Electromagnetic processes

The $\overline{\text{P}}$ANDA detector represents a typical 4π-device which allows the nearly complete detectioni of all charged reaction products as well as primary and secondary γ-rays. Since $\overline{\text{P}}$ANDA is a fixed target experiment the momentum boost of all rection products is compensated by a target and a forward spectrometer, respectively. Both comprise several detector layers for tracking, particle identification and energy measurement, in case of electromagnetic probes. [Col08]

Therfore the electromagnetic calorimeter (EMC)is one of the main components in the target spectrometer of $\overline{\text{P}}$ANDA and hast to provide sufficient in energy resolution and sensitivity for photon and meson spectroscopy over the relevant energy region. The EMC design has to fulfill strong requirements in order to provide successful operation during the experiment. The main requirements are

- Geometrical coverage close to 4π

- Precise energy and position reconstruction with high resolution over an energy range of $10MeV$ to $15GeV$

- Good time resolution for event identification

- Fast response to accomplish high count rates due to the annihilation rate $\sim 10^7 s^{-1}$

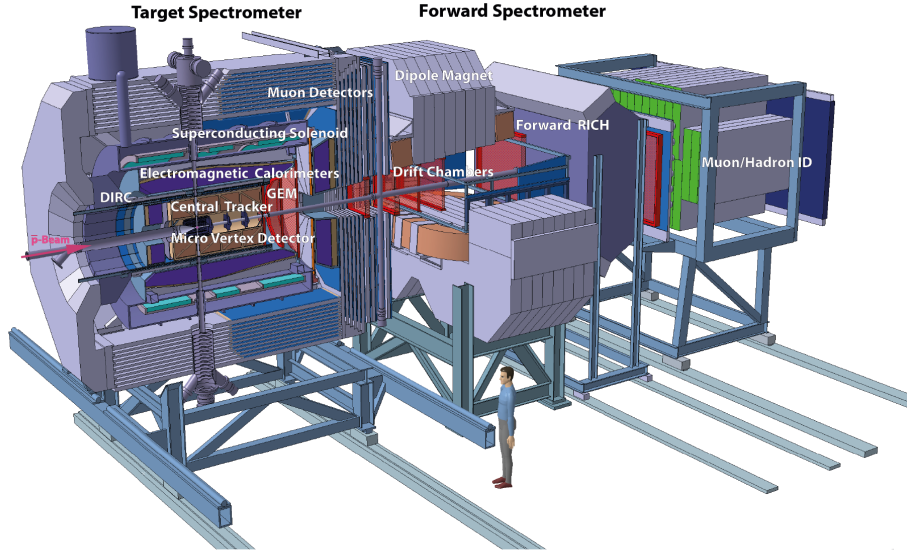- Compactness to be installed inside the solenoidal magnet

- Radiation hardness

Figure 1.2: Overview of the planned $\overline{\mathrm{P}}$ANDA detector [Col08].

In the following section the physical goals of $\overline{\mathrm{P}}$ANDA as well as the requirements for the EMC will be discussed iin more detail. The radiation hardness is the main topic of this thesis.

1.1 Physics Program

Quantum Chromo Dynamics (QCD)
QCD the approved quantum field theory of quarks and gluons being an established part of the standard model of particle physics still poses challenging questions, even decades after the first proposal. While being well understood and tested in the high energy regime, where the coupling constant α_s is small and perturbation theory applies, this is not the case for the low energy regime. This strongly-coupled non-perturbative regime still holds many non understood aspects. This limited knowledge is the major driving forces of the physics program of $\overline{\mathrm{P}}$ANDA.

Charmonium spectroscopy
In the non-perturbative region QCD predicts a lot of different excited Charmonium states (quark content $c\bar{c}$). This region will be fully accessible for $\overline{\mathrm{P}}$ANDA. It is the perfect tool for experimental testing of these predictions. Lattice-QCD opened up a new way to compute and predict these states with high precision as illustrated in Fig. 1.3. To further understand the theory measurements of existing states with high precision are mandatory. While charmonium has been widely experimentally studied

since its discovery of J/ψ in 1974 most experiments relied on e^+e^- annihilation, where direct charmonium production is possible only for states with the quantum numbers of the photon $J^{PC} = 1^{--}$. All other states have to be populated via secondary decays. Using $p\overline{p}$ reactions for charmonium productions all states can be directly formed. The resolution in this case relies on the beam quality. The HESR will be able to descretely scan the energy region leadingto resolutions of the measured masses in the order of 100 keV as shown in Fig. 1.4.
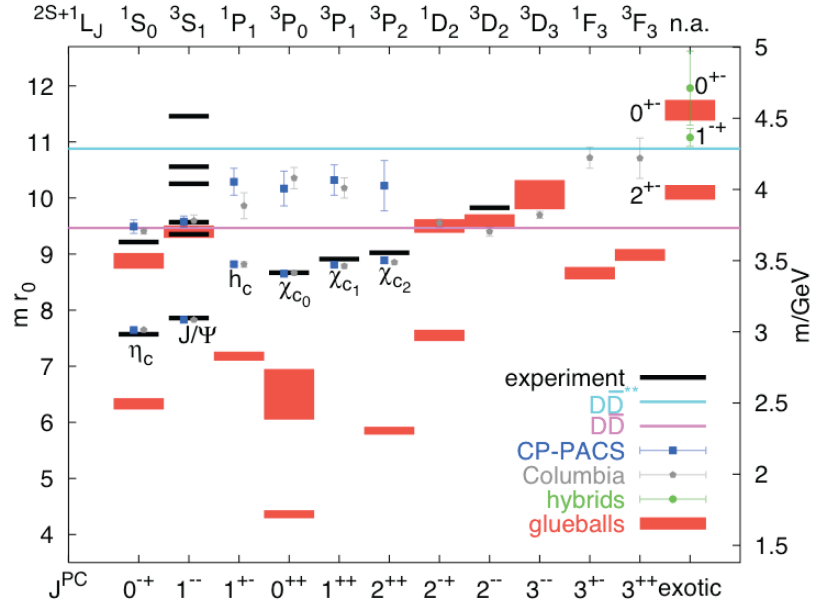

Figure 1.3: Lattice-QCD predictions for the charmonium, the glueball and the spin exotic $c\overline{c}$-glue hybrids spectrum in quenched Lattice-OCD.

Search for gluonic excitations

QCD predicts the existence of different gluonic excited states. In general, these divide into two groups, glueballs i.e pure gluon states and hybrids consisting of $q\overline{q}$ and an excited gluon. The additional degrees of freedom carried by these hybrids and glueballs allow for exotic quantum numbers J^{PC}, whereas these are not possible for standard $q\overline{q}$ configurations. Relying on exotic quantum numbers poses the advantage to detect glueball spectra which do not mix with the neighboring $q\overline{q}$ states leading to easier experimental identification. Thus avoiding uncertainities such as in the cas of studies with the Crystal Ball at LEAR[5] (CERN [6]) where the $f_0(1500)$ resonance was found to be a strong glueball candidate, but could not be isolated due to the mixing of the $J^{PC} = 0^{++}$ ground states.

---

[5]LEAR = L̲ow E̲nergy A̲ntiproton R̲ing
[6]CERN = C̲onseil E̲uropéen pour la R̲echerche N̲ucléaire
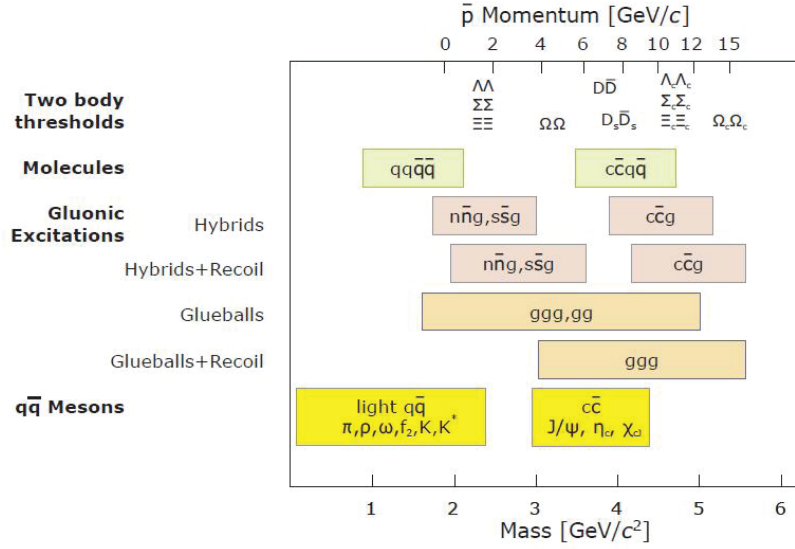
Figure 1.4: Accessible mass range with $\overline{\mathrm{P}}$ANDA (below) with respect to the required antiproton momentum (above)[Met08].

Given the proposed beam energy and the use of $p\overline{p}$ annihilations this provides a favorable environment for the spectroscopy of gluonic excitations to gain deeper insight in the QCD vacuum.

[7]

Investigation of hadron properties inside nuclear matter

To fully understand the origin of masses in hadronic matter one has to research the in-medium-modifications of the embedded hadrons. So far this research focused on the light quark sector, whereas $\overline{\mathrm{P}}$ANDA with the 15 GeV antiproton beam can investigate the charm sector.

Hypernuclei

Introducing strangeness into the nucleus one has to replace an existing up- or down-quark with a heavier strange quark. The result is called a hypernucleus opening up a new degree of freedom on the known nuclear chart illustrated in Fig.1.5. With the antiproton beam the experiment will be able to produce hypernuclei in a with an efficiency comparable comparable to dedicated experiments. New insight of the inner structure and forces of hyperons and nucleons will be gained by that approach.

Electromagnetic processes

As a different approach to the investigation of nuclear structures one can study electromagnetic processes. $\overline{\mathrm{P}}$ANDA will provide this additionally to the main research

---

[7]CERN = $\underline{C}$onseil $\underline{E}$uropéen pour la $\underline{R}$echerche $\underline{N}$ucléaire

Figure 1.5: Artistic view of the hypernuclear chart)[Met08].

field of spectroscopy. Like the reaction $p\overline{p} \rightarrow e^+e^-$ could lead to better determination of the electromagnetic form factors of the proton. On the other hand electromagnetic processes such as wide angle compton scattering will be accessable.

1.2 The Importance of the Electromagnetic Calorimeter

One common feature of all the physics topics to be studied with the $\overline{\text{P}}$ANDA detector is that in most reactions the final state consists of several photons and electrons/positrons. This puts the electromagnetic calorimeter (EMC) into special focus. It is the only device to measure energy directly by detecting photons with high efficiency over 99 % of the solid angle. All the performance parameters have to be tuned to the requirements of the experiments.

In case of $\overline{\text{P}}$ANDA the energy threshold and the dynamic energy range become crucial. Having sufficient background rejection to distinguish effectively for example charmonium decays from background events every single photon has to be detected e.g. in Fig. 1.6. Maximizing the acceptance of low energy photons a minimum energy threshold

$E_{thresh} = 10\,\text{MeV}$ should be reached. On the other hand an energy range up to $15\,\text{GeV}$ has to be considered. The low energy threshold is mandatory for all parts of the EMC while the projected highest energy only has to be covered by the forward endcap in upstream direction of the beam. The projected energy ranges for the different parts are:

Backward endcap	10 MeV - 0.7 GeV
Barrel	10 MeV - 7.3 GeV
Forward endcap	10 MeV - 14.6 GeV

The individual detector module gas to allow a low energy threshold of $1 - 2MeV$ for shower reconstruction. Apart from being able to detect all particles a good energy
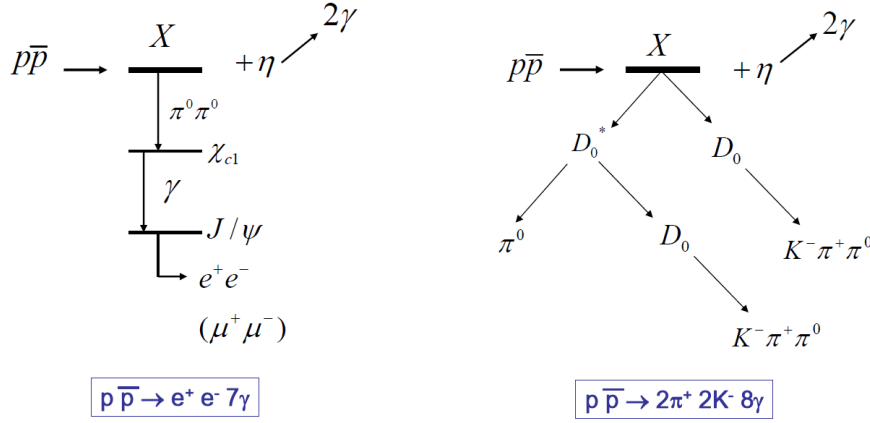
Figure 1.6: Possible decays of a hybrid state X, the only difference in the final state after the decay of all pions is one photon. (left: 7 photons / right: 8 photons)[Met08].

resolution has to ensure the exclusiveness of events, as well as delivering high precision $\frac{E}{p}$ values. This is necessary to distinguish e^- and e^+ from π. Therefore the energy dependent resolution parameterized by

$$\frac{\sigma_E}{E} = a \oplus \frac{b}{E[GeV]} \tag{1.1}$$

has the requirement of $a \leq 1\%$ and $b \leq 2\%$. The first parameter quantifying the shower leakage or uncertainities of calibration, the latter one relying on the photon statistcs. Due to domination of the constant term the resolution limit for high energies is set to $\frac{\sigma_E}{E} \leq 1\%$.

For the angular coverage of the EMC a 4π solid angle is envisaged excluding the hole in the forward endcap to allow passage of particles with an extreme forward boost. This part will be covered by a shashlik calorimeter. The backward and forward part of the

EMC will be covered by two endcaps, while the barrel will surround the target and the beampipe at a radius of 57 cm (Fig. 1.7). A total of 15552 single crystals is required for the build, 11360 for the barrel, 3600 for the forward and 592 for the backward endcap respectively. All these have to meet high fabrication and quality standards to achieve homogenity throughout the whole EMC. The overall compactness is required due to high production costs of the scintillators and the surrounding magnets, which scale with the third order of the volume. Using single crystals with a frontface in the order of $4\,\text{cm}^2$ ensures excellent position resolution of the EMC. This position resolution is required for the reconstruction of the invariant mass of primary particles. The reconstruction relies on precise knowledge of the point of impact of these particles. It is achieved by weighing the electromagnetic shower extending over a cluster of crystals and finding the center of gravity.
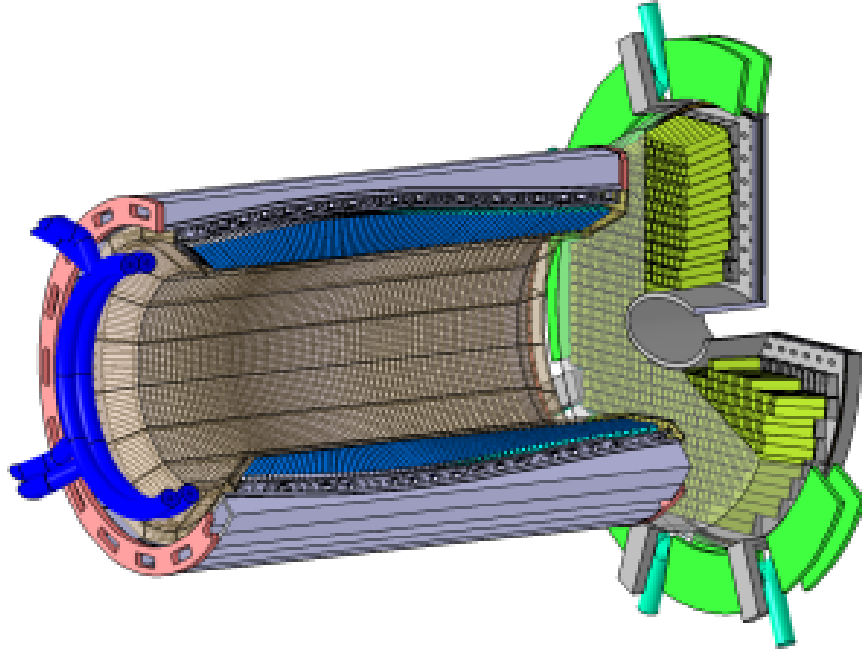
Figure 1.7: A CAD drawing of the planned EMC for $\overline{\text{P}}$ANDA without the backward endcap [Col08].

Taking into account the high luminosity of the $\overline{\text{P}}$ANDA experiment reaching a maximum at $2 \cdot 10^{32}\,\frac{1}{\text{cm}^2\text{s}}$ the EMC has to handle the high count rates. The projected hit rates per crystal are $\approx 60\,\text{kHz}$ for the barrel part and $\approx 500\,\text{kHz}$ for the forward endcap (Fig.1.8) The time resolution is limited mainly by the risetime of the scintillation material and the electronics. A time resolution $t_0 \leq 1\,\text{ns}$ is envisaged in order to define a clean time stamp of the individual signal for event reconstruction in the triggerfree DAQ concept. The rate capability depends on the decay time and the shaping of the signal in the electronics in order to minimize pile-up.

The last and one of the most important requirements for the overall success is the
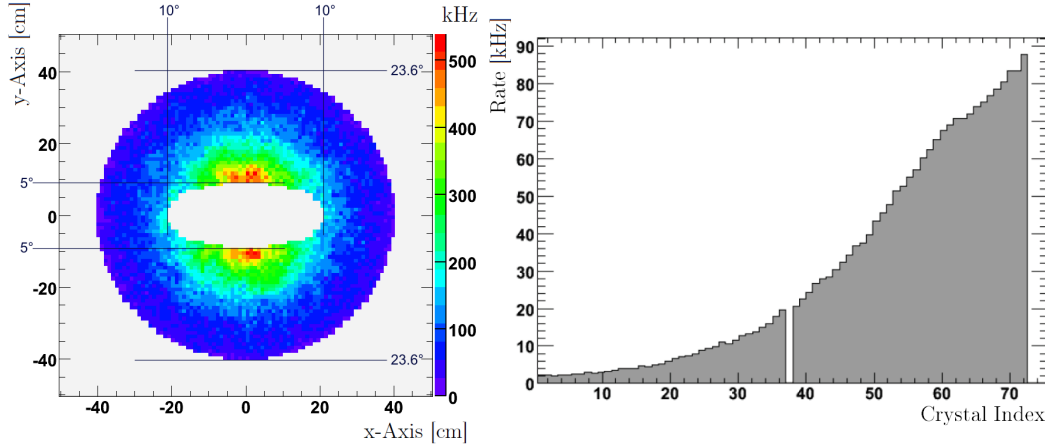
Figure 1.8: Simulation of the maximum hit rates with a beam momentum of 14 Gev for the forward endcap (left) reaching the maximum next to the beampipe and for the barrel (right) the crystal numbers corresponding to the position in the barrel, i.e. in beam direction from 0 to 72[Col08].

radiation hardness of scintillator material. The envisioned runtime of $\overline{\mathrm{P}}\mathrm{ANDA}$ will be 10 years in factory-mode, i.e. 9 month runtime followed by 3 month for maintenance and repairs. To ensure high precision measurements for the whole time every component has to be as radiation hard as possible. The accumulated dose would be $\leq 125Gy$ per year for the most forward crystals and two magnitudes lower for the barrel and backward endcap crystals. The performance of all known crystal scintillators suffers from radiation damage. The damage depends on the type of particle and its energy. The most common phenomena for γ-radiation are the creation of color centers and phosphorescence. The first leads to additional absorption bands in the crystal structure shortening the absorption length hence reducing the light output, as illustrated in Fig. 1.9. The latter one is generating an afterglow and increasing the readout noise level. Hadrons on the other hand can directly interact with the crystals structure, changing nuclei through capturing processes or damaging the crystal structure and influencing the scintillation mechanism directly. All these processes change the measured light output and inluence a stable operation. Most of these damages can be thermally annealed. At room temperature the γ-radiation induced damage and the relaxation can reach an equilibrium depending on the dose rate. On the other hand the thermodynamical nature of the recovery processes changes completely when the crystals are cooled to significantly lower temperatures.

For the reason of increasing the light yield of the EMC the foreseen operation temperature will be T = -25°C. Making it even harder to maintain stability of the scintillation parameters and requiring for extensive calibration throughout the runtime.

The material of choice for the scintillation crystals is $PbWO_4$ -lead tungstate- naturally found as the tetragonal stolzite or monoclinic raspite. $PbWO_4$ (PWO) as a
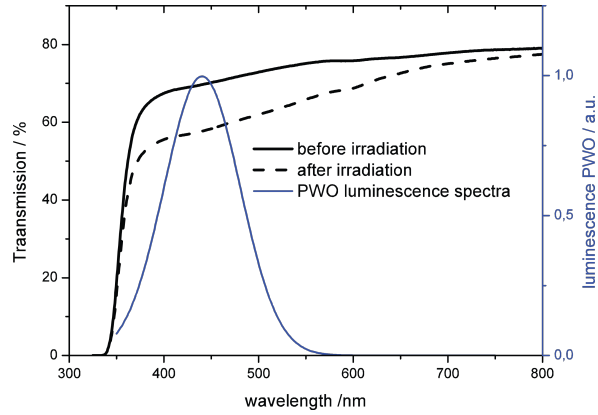
Figure 1.9: Change of optical transmission for PWO-II crystal after irradiation with 30Gy (in blue the luminescence spectra is shown)[Col08].

scintillator provides the required fastness, compactness and radiation hardness. The high density of $8.28\,\frac{g}{cm^3}$ leading to short radiation length $X_0 = 0.89\,cm$ and a Moliere radius of $R_M = 2.1\,cm$, thus allowing the compact design. Apart from this, the decay time of the main luminescence center at 420 nm as seen in Fig. 1.9 is sufficiently fast. PWO is also used in the CMS[8] experiment at CERN, which established fabrication processes considering stable quality and homogeneity in the mass production of these crystals. A huge R&D program has been undertaken to further improve all the parameters of PWO fine tuning them to the needs of $\overline{P}$ANDA. Better selectioin of the raw material and improvement of the growing technology succeded in reducing the concentration of defects. Therefore one could reduce the doping concentration of Lanthanum and Yttrium ions by a factor two, which improved the light output, characterized as PWO-II. This type of crystals have a 80% higher light yield compared to the CMS-type crystals and by cooling them down the yield can be further increased. Concluding in a factor eight at T = -25°C compared to the lightyield of CMS-type crystals at room temperature. So far 50% of the total amount of crystals have been supplied by BTCP[9] which was the manufacturer as well for the 77000 crystals of the CMS-ECAL calorimeter.

---

[8]CMS = Compact Muon Solenoid
[9]BTCP = Bogoroditsk Techno Chemical Plant

1.3 The scintillation process of lead tungstate

1.3.1 General aspects

From the first experimental use of the scintillation mechanism in the 1940s to present-day experiments, scintillators, organic or inorganic, have made a huge impact on high energy physics. Nowadays electromagnetic calorimeters are one of the most important parts of all major experiments. In general, scintillators serve two purposes in an experimental setup, the main purpose is to convert energy, deposited by traversing high-energy particles, into light, the second purpose is to guide that light to a photon sensor.

Not to confuse scintillation with other effects exhibiting luminescent behavior (e.g. lasers), the origin of scintillation is always the energy loss of ionizing radiation in matter. While traversing matter neutral particles and charged hadrons interact directly with nuclei producing secondary charged particles or via ionization in case of charged particles. On the other hand, γ-quanta lose their energy mainly through three fundamental interactions:

- photoeffect

- compton scattering

- electron-positron pair production

The interaction cross section of these processes is energy dependent. For small energies in the keV-region photoabsorption proves to be dominant as is the compton scattering the dominant process in the medium energy region. For high energy experiments the electron-positron pair production is the relevant process starting at an onset of 1.02 MeV, the mass of an electron-positron pair at rest. The emitted high energetic leptons reduce their energy over the distance X_0, the radiation length, by a factor $1/e$. The mean free path of pair production amounts to 7/9 X_0. The radiation length for a given material can be approximated by the following equation

$$\frac{1}{X_0} = 4\alpha r_e^2 \frac{N_A}{A} \left(Z\left(Z+1\right) ln\frac{287}{\sqrt{Z}} \right) \tag{1.2}$$

where Z is the atomic number and A is the mass number of the nucleus.

If the energy of any of these secondary electrons or positrons exceeds the critical energy

$$E_c = 550 \frac{\text{MeV}}{\text{Z}} \tag{1.3}$$

they will lose energy by emission of bremsstrahlung. Hence creating new photons which interact in the same ways as the incident photon [ea11].

If the energy of the incident electromagnetic probe is high enough, this energy is progressively distributed in multiple scattering processes auch as pair-production and bremsstrahlung leading to low energetic electrons or photons, which are finally absorbed after ionization or photo effect forming an EM shower. Furthermore nuclei of the matter excited or ionized by neutral particles or charged hadrons will relax and emit γ-quanta and electrons to the mix. These again lose energy with the interaction processes described above. The electrons created by this process will continue to lose energy and in the case of a crystal start to interact with the atoms and electrons from the lattice by creating electron-hole pairs in the material. If the energy exceeds the ionization threshold the electron and the hole will be free to travel inside the crystal lattice either recombining on a luminescent center or being trapped by any defect. Below the ionization threshold the charge carriers will couple to the vibrational modes of the lattice and vanish into the conducting or valence band. To be a scintillator the material must contain luminescent centers, which are either inherent to the material or being added in the creation. To emit light these centers possess radiative transitions between excited and lower states. The energy levels of all these transitions have to be in the forbidden zone between the conduction and valence band to prevent reabsorbtion or photo-ionization of the center.

1.3.2 Lead tungstate scintillation mechanism

Deducing from the electron band structure of PWO luminescence appears in PWO crystal because of charge-transfer transitions in anionic molecular complexes. The WO_4^{2-} complex being the main source for the intrinsic blue luminescence. In this anionic complex the spin and parity forbidden radiative transition $^1T_1$, $^1T_2 \rightarrow^1 A_1$ to the ground state is responsible for the 420nm emission. The irregular WO_3 complexes contribute to the scintillation with different transitions but the blue luminescence becoming the dominant one at room temperature. This effect is further enhanced due to optimized growth conditions and further purification of the raw materials.[AKL02, Col08, LDA$^+$95] Naturally found PWO is almost always non transparent and yellowish in color. The optimized growth conditions lead to the transmission spectrum nearly reaching the theoretical maximum enabling the use of PWO as a scintillator. The other characteristic of PWO is low light yield and the fastness of the scintillation decay, both arise from the strong thermal quenching. This means, non-radiative transitions back into the ground state of the electron appear mostly due to phonon coupling in the crystal lattice. The stokes shift, which is a measure of the interaction between the emitting center and the vibrating lattice is rather large for WO_4^{2-} with a value of 0,44eV. This being the reason for the extremely low light yield of PWO at room temperature. Cooling the crystals reduces the amount of non radiative recombination giving rise to the photon emitting transi-
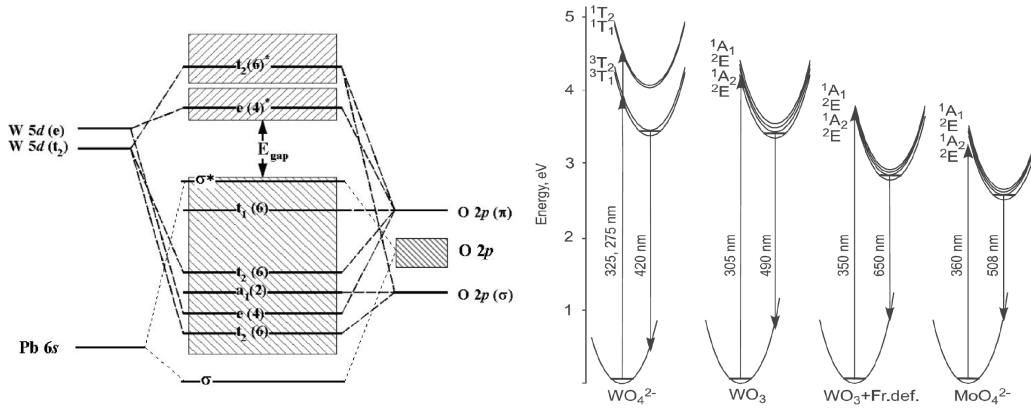
Figure 1.10: Left: Schematic molecular orbital diagram for W-O and Pb-O interactions superimposed on blocks representing calculated PbWO4 valence and conduction bands.[WZAH99] Right: Radiative charge-transfer transitions responsible for the luminescence [AKL02].

tions. The strong thermal dependence demands precise temperature stability for the experiments.[LDA+95, Col08, LAG+06]

1.4 Radiation Damage and Recovery

1.4.1 General Aspects

Scintillators as a detector for ionizing radiation are forced to operate in hostile radiation environments. A mandatory requirement is the stability of their parameters under the influence of ionizing radiation. The most common criteria by which the radiation hardness is measured is the change of detector scintillation efficiency when exposed to different kinds of radiation, for example the reduction of the light yield. Considering all the different aspects on which efficiency reduction depends, like the integral dose, dose rates, storage conditions, types of radiation, recovery, etc., it is impossible to generalize the radiation damage by just the reduction of efficiency. It is necessary to individually study the deterioration mechanisms for each scintillator type. The knowledge of these mechanisms is of great importance to ensure calibration and stability of the EMC in the experimental run.

Most commonly radiation damage manifests in the loss of transparency of the material. Usually this is caused by the formation of color centers thus reduciing the attenuation length. This process of self absorption does not affect the amount of produced photons per MeV it only reduces the efficiency of photon transport towards the photodetector. Another mechanism could be the modification of the luminescence centers thereby

reducing the luminescence yield and changing the homogeneity of the crystals. Finally phosphorescence or afterglow of the crystals can increase the background of the signal. Furthermore, hadrons can damage the whole crystal by displacing or changing the nuclei in the crystal lattice. This would not only affect light transportation, but the luminescence itself. Opposed to the damage done by ionizing radiation this might not be easily annealed by heating or UV bleaching, which is the case for most non hadronic damages.

The $\overline{\text{P}}$ANDA experiment relies on PWO which has been studied quite well for the last decade. It has been shown that the scintillation mechanism remains very stable and is not affected under radiation even for high energy hadrons. PWO radiation damage consists solely on the appearance of absorption bands due to color center formation. [yZ98, **?**, PL06]

This leads to the main quantifying parameter for radiation hardness the loss of transmittance. It is derived from the Lambert-Beer law as shown here:

$$T = e^{-k \cdot d}. \tag{1.4}$$

where T is the transmission, d is the pathlength and k is the absorption coefficient. Assuming the radiation induced change of transmittance is purely exponential this leads to an easy way to quantify this losses by the parameter Δk normally expressed in m^{-1}.

$$\ln \frac{T_b}{T_a} = \ln \frac{e^{-k_b \cdot d}}{e^{-k_a \cdot d}} = d(k_a - k_b) = d \cdot \Delta k. \tag{1.5}$$

$$\frac{1}{d} \cdot \ln \frac{T_b}{T_a} = \Delta k. \tag{1.6}$$

T_a and T_b is the transmission before and after irradiation, d is the pathlength and Δk is the difference between the absorption coefficient before and after. In addition this coefficient is as always wavelength dependent. [**?**]

1.4.2 Color Centers in PWO

Different kinds of color centers are known to exist depending on the type of the defects in the crystal. Color centers may be electrons located in anion vacancies (F-center), or holes located in cation vacancies (V-center), or interstitial anion atoms (H-center) or ions (I-center). The creation or annihilation of these radiation-induced color centers may be observed by measurement of crystal's transmittance. [yZ98] The F-center and its antimorph the V center are always created in unison owing to the overall neutral structure of the crystal. The F-center being the simplest trapped electron center. It has been identified by means of EPR studies as an electron bound to a negative ion vacancy. The optical absorption of the F-center is characterized by the crystal and
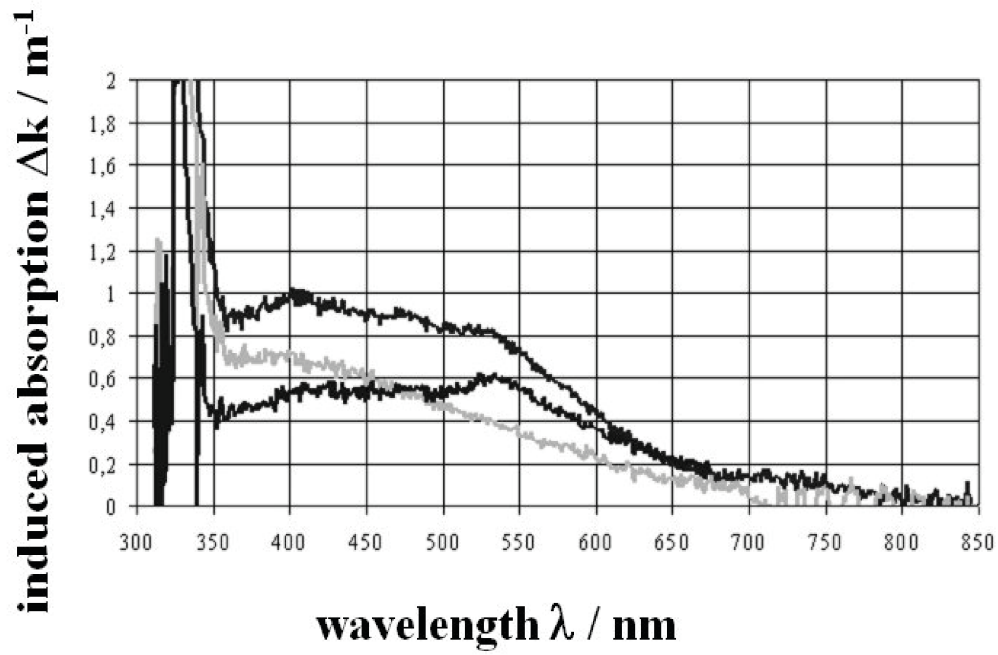
Figure 1.11: The measured change of the induced absorption coefficient of various PWO-II samples after irradiation with a dose of $0.2kGy$ (^{60}Co) over the relevant range of wavelength. [Col08]

exists due to an electric dipole transition to a bound excited state of the center. On the other end, the V-center is a hole trapped at a positive ion vacancy. V-centers have been shown to behave like molecular ions. More complicated centers are formed when F-centers neighbour each other. The M-center consists of two F-centers and R-center of three F-centers. All these centers can be distinguished by their optical absorption frequencies.[Kit96]

In PWO crystals several metastable color centers have been found. By means of Electron Paramagnetic Resonance (EPR) measurements after consequently filling of the traps through X-ray irradiation three characteristic centers are observed. The depth of these is characterized by the energy gap towards the valence band as shown in figure 1.12. The shallowest one is an intrinsic defect; via Jahn-Teller distortion
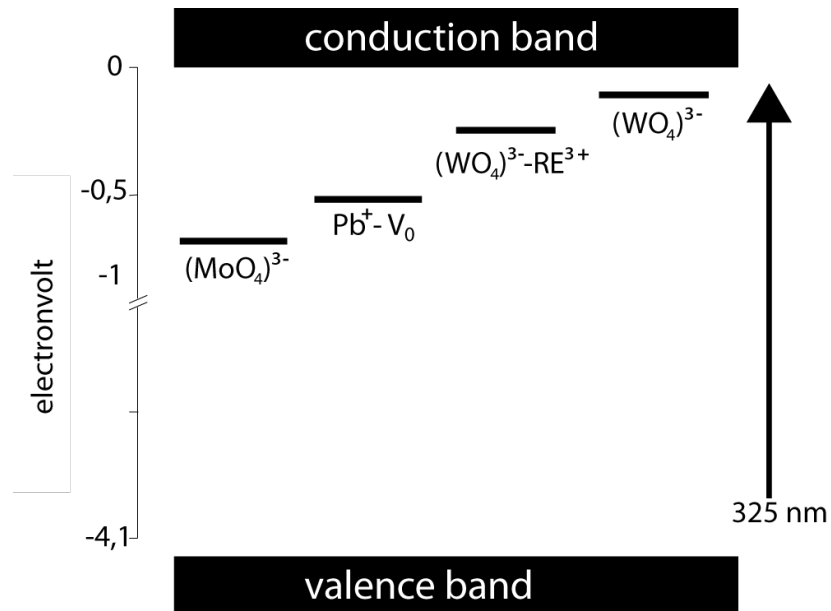
Figure 1.12: Identified electron traps ind PWO. [Hof10]

the $(WO_4)^{3-}$ polaronic center from an anionic $(WO_4)^{2-}$ complex is created with an additional electron. This trap has an activation energy of $50meV$ and is emptied at $50K$. The released electrons partly recombine radiatively, and partly are caught by deeper traps.

The second center is Pb^+-V_0, it is an F-center and stable up to $175K$. The electron is trapped in the vicinity of an oxygen vacancy and has an activation energy of $90meV$
The third F-center is $(WO_4)^{3-}$ and originates from a regular tungstate anionic complex deformed by rare earth (Re) impurity ions like La, Lu or Y. It is stable up to $97K$ and the activation energy is between $190 - 200meV$. The doping process with trivalent

rare earth in concentrations of tens of ppm reduces the number of deep traps by an overall redistribution of them.

Other deep paramagnetic F-centers are created by $(MO_4)^{2-}$ complexes, which replace tungstate groups at regular spots thus preserving the lattice symmetry. With an additional electron these create $(MO_4)^{3-}$ which are metaststable even above room temperature. While the $(MO_4)^{2-}$-center shows green luminescence and slow scintillation decays, the $(MO_4)^{3-}$-trap creates an absorption band with a maximum near 530 nm.

Studies have shown that there are no intrinsic defects based on cation or anion vacancies with a paramagnetic groundstate in PWO. This leads to the assumption that separate F^+ centers (anion vacancy $(V_0)^+e$) and O^- have no energy levels in the forbidden zone. Concluding the only metastable color centers under irradiation are cation vacancies capturing two holes of the type $O^-V_cO^-$ and oxygen vacancies or their associates amassing the electron capture. One can infer the existence of a variety of traps in undoped and doped PWO with approximate activation energies of 50, 70, 130, 200, 210(230), 270, 400, 490, 500, 580 and 700 meV. The nature of traps which were not observed directly with EPR remains a matter of discussion. The 70 meV trap is detected in all measured samples, however it disappears in the samples grown in an oxygen-rich atmosphere. In crystal with rare earth doping another 130 meV trap center appears. It is not paramagnetic and probably related to RE-$(WO_4)^{4-}$ capturing two electrons. If one of the electrons is released from these traps it is subject to immediate retrapping creating centers with even lower energy, as well as creating RE-$(WO_4)^{3-}$. This hypothesis is well backed up by TSL measurements. In accordance with the luminescence spectra the deepest observed electron trap is attributed to (WO_3) distorted by a Frenkel defect, the V_0 vacancy is responsible for the trapping of electrons. Such a center appears under irradiation, is stable at room temperature and shows absorption spectra close to the (WO_3) center near the Frenkel defect. All of the deepest F-centers are attributed to anionic tungstate complexes. These centers have the main absorption band between 350-400 nm [AKL02, QD99]

1.4.3 Radiation Damage and Recovery at Room temperature

If all the radiation damage in PWO originates in the creation of color centers and the damage to the scintillation mechanism is negligible.there is a constant annihilation process of the color centers at roomtemperature. Leading to some kind of equilibrium of creation and annihilation of color centers for low dose rates. In Figure 1.13 it is shown that the PWO transmission damage reaches a saturation level, which is dose-rate dependent up to the point where spontaneous relaxation and damage creation equal each other. When the irradiation process ends the color centers annihilate through different effects. Normally this effect is described by the combination of two
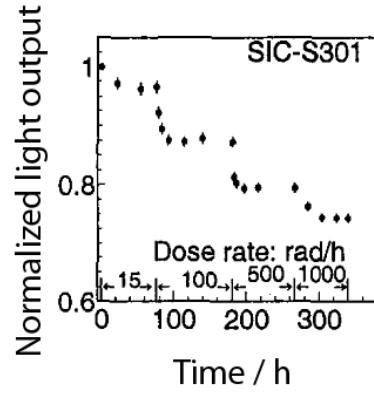
Figure 1.13: Normalized light yield as a function time and doserate [XDQC00].

exponential functions, taking into account that not all centers decay through fast thermal activation but rather via electron/hole recombination through tunneling of the electron. The difference between the fast and the slow component can be seen
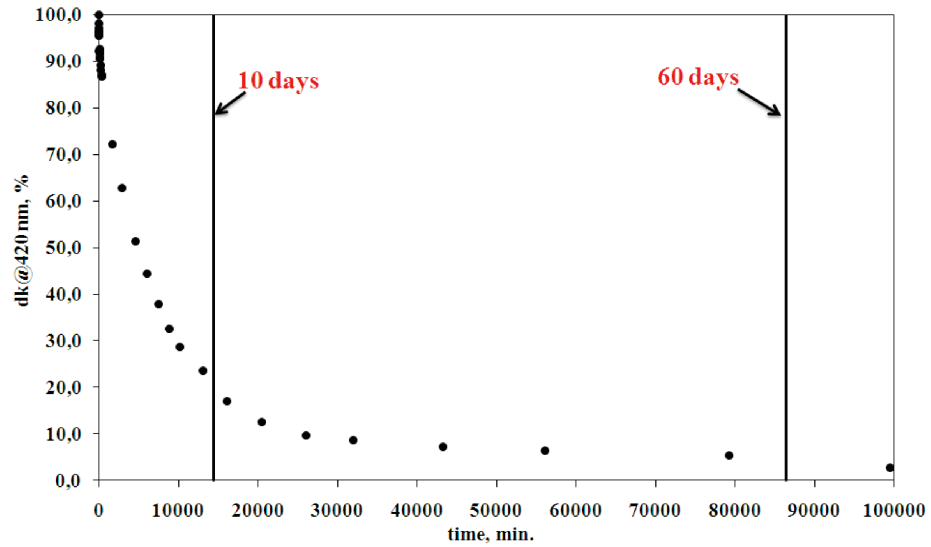
Figure 1.14: Spontaneous recovery of Δk at room temperature as a function of time [Dor].

in figure 1.14. The recovery of the first 50% take roughly 5 days, while the it takes around 70 days to recover the remaining 50%.

In recent experiments is has been shown that the recovery can be severely speed up by the application of light, so called stimulated recovery. For room temperature this delivers impressive results.
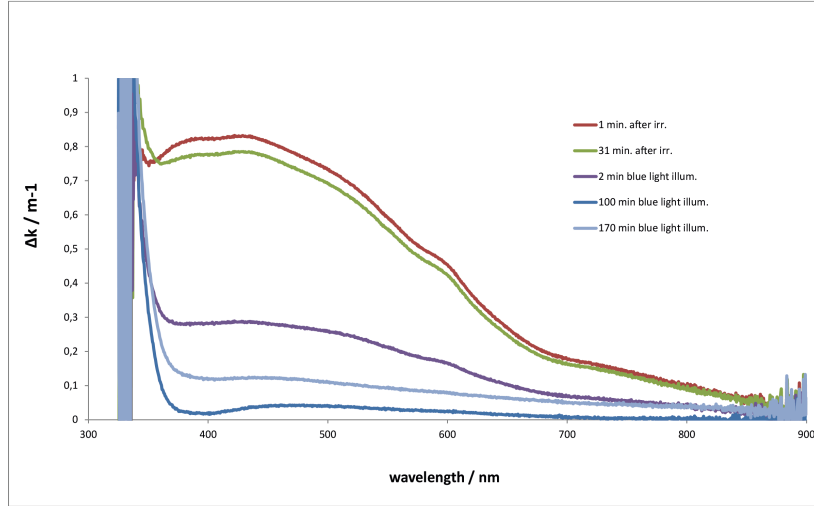
Figure 1.15: Radiation induced absorption spectra of the full size (20 cm) PWO-II crystal illuminated with 464 nm [Dor].
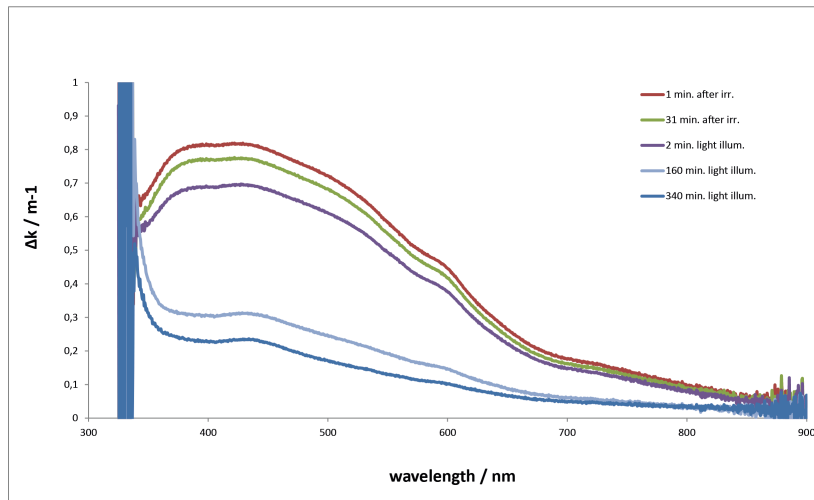
Figure 1.16: Radiation induced absorption spectra of the fullsize (20 cm) PWO-II crystal illuminated with 1060 nm [Dor].
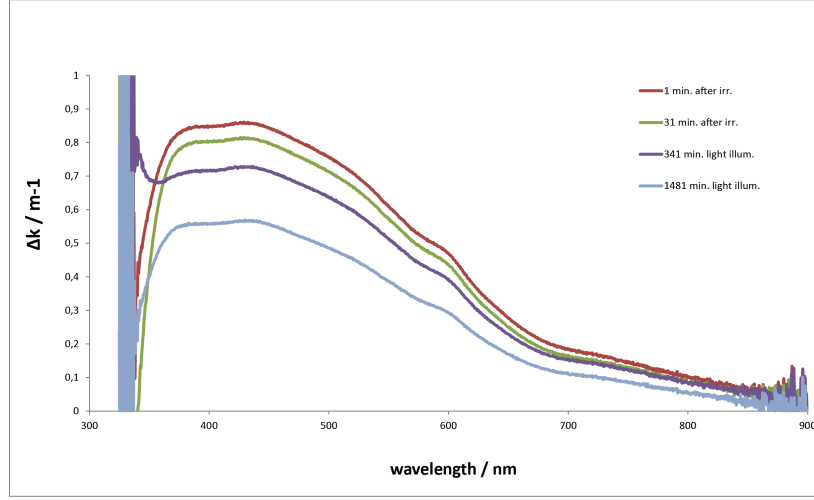
Figure 1.17: Radiation induced absorption spectra of the full size (20 cm) PWO-II crystal illuminated with 1550 nm [Dor].

All the crystals were irradiated with $30Gy$ and illuminated afterwards with light of different wavelength. It can be clearly seen in figures 1.15, 1.16 and 1.17 that the radiation induced absorption described by Δk recovers at a fast rate.

In Fig. 1.18 it can be seen that the stimulated recovery process works in a very wide wavelength regime. It is even useful in the greater infrared region. The timescales for recovery shrink by a factor of 1000 compared to the spontaneous recovery via the thermodynamical relaxation processes only. (Table 1.4.3)

wavelength / nm	464	940	1060	1300	1550	spont. recovery
time of 90% recovery / min	23	370	1150	3060	9100	2600

To apply that process to $\overline{\mathrm{P}}$ANDA would significantly stabilize the long term operatin of the calorimeter.

1.5 Radiation Damage and Recovery in Cold PWO-II Crystals

At room temperature there is a continuous annihilation process of the color centers. Leading to an equilibrium of creation and annihilation of color centers for low dose rates. However for the $\overline{\mathrm{P}}$ANDA experiment it is foreseen to operate at $T = -25°C$, therefore the damage and spontaneous recovery for cool crystals is of great importance.
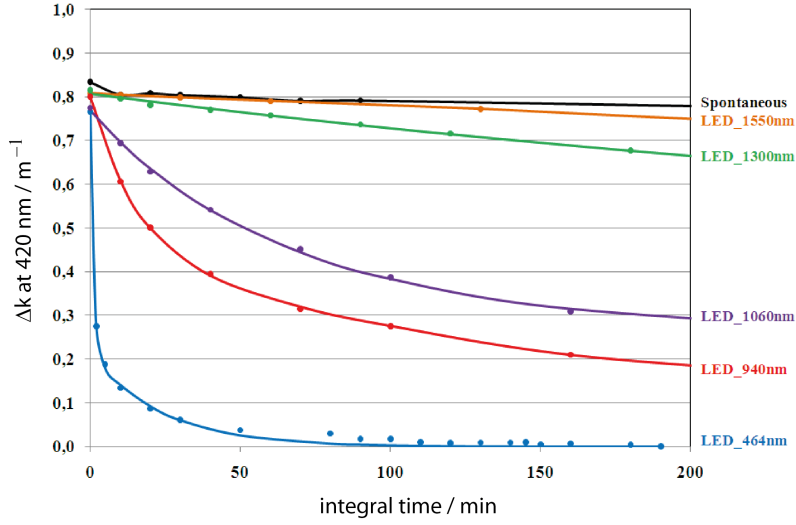
Figure 1.18: Stimulated recovery of $30Gy$ radiation damage in PWO at room temperature.

Studies at $T = -25°C$ have shown, that not only reaching of the equilibrium level is dose rate dependent and significantly lower but the spontaneous recovery seems to be nearly frozen. The decline of thermo-activated relaxation shows that the saturation level is much lower and the saturation level is not reached even after hundreds of hours irradiation with $0.2Gy/h$. [ea07] Figure 1.20 shows the very slow recovery for two crystals at low temperatures compared to room temperature recovery. One has to heat up the crystals to room temperature or higher before one can expect recovery on a reasonable timescale.

The practical nonexistence of spontaneous recovery at low temperatures imposes the long relaxation pause every year onto the run schedule just to heat up and recover for a long period and one has to cope with significant transparency losses during operation.

1.6 Open questions

Taking into account the huge impact of stimulated recovery at room temperature towards stability and efficiency of a given PWO detector module. It should be studied if the mechanism can be applied at low temperatures. For an application in the EMC of $\overline{P}$ANDA it has to be studied at $T = -25°C$.
The investigation has to focus on the timescale for recovery, the necessary photon flux and the range of wavelengths of the external light source. In addition, the mechanism
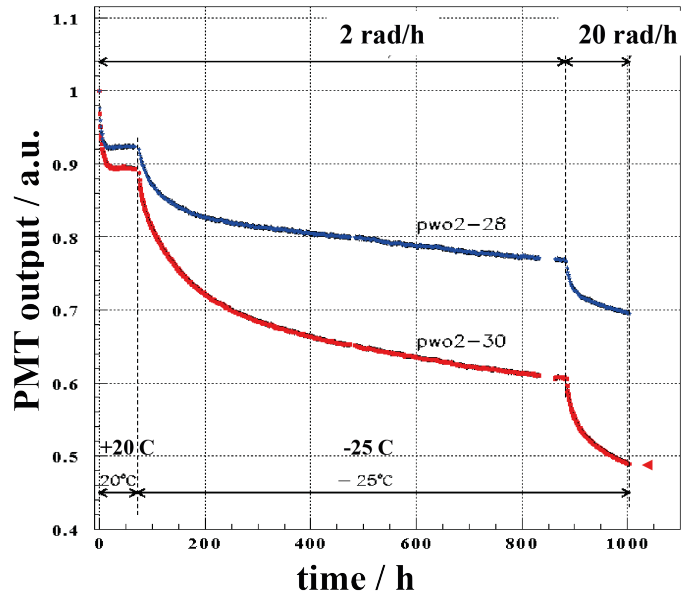
Figure 1.19: Dose rate dependency of signal loss for two cooled PWO crystals [ea07].
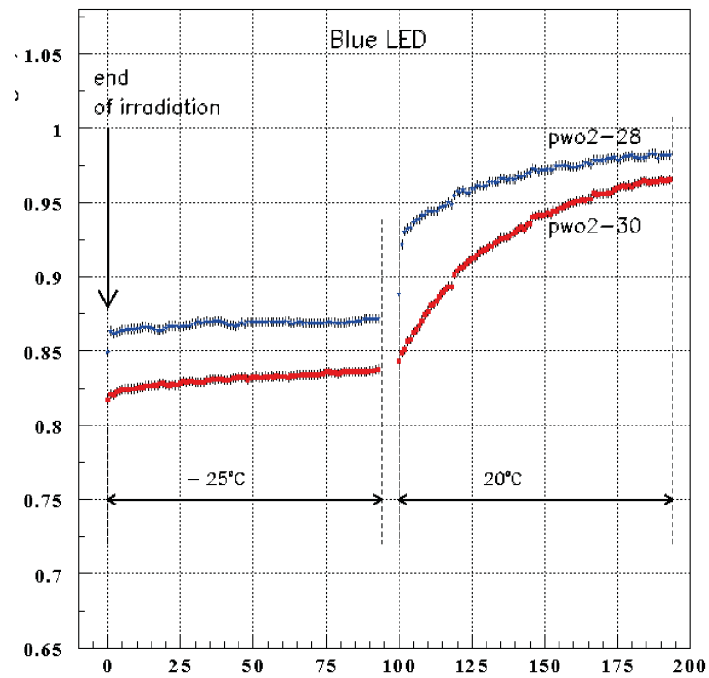
Figure 1.20: Left: recovery of transmission at $T = -25°C$ right: recovery of transmission at room temperature) [ea07].

might be limited to specific color centers. This can be done by quantitative studies at low temperatures. Therefore, EPR and transmission measurements become mandatory to describe the mechanism even in a model. All this has to be done to elaborate a technical concept for any kind of application in $\overline{\mathrm{P}}$ANDA.

The next question which arises is the application of stimulated recovery in situ when irradiating the crystal. This approach would not only avoid dedicated recovery phases between experiments, but could prevent the transmission loss in general. The optical
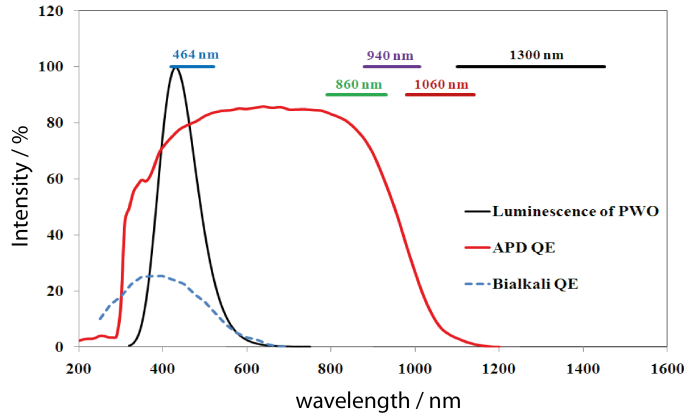
Figure 1.21: Luminescence of PWO with the wavelength dependent quantum efficiency of the foreseen detectors. Superimposed is the wavelength distribution of different LEDs used in stimulated recovery experiments [Dor].

sensitivity of the used LAAPDs and vacuum phototriodes as sensors provide the possibility to recover the radiation damage on line during the experimental run, see Fig. 1.21 Furthermore, the wavelength dependency suggests the use of shorter wavelength for off line recovery in between production runs and on line recovery oif the photo sensor is blind for the external light source.

To conclude, the target of this thesis is to address and answer the following questions:

- Is stimulated recovery working at $T = -25°C$?

- What are the differences with respect to the room temperature recovery?

- What kind of color centers are affected by stimulated recovery?

- On-line or off-line recovery as a technical proposal?

Chapter 2

Stimulated Recovery of Radiation Damage at Low Temperatures

2.1 The Cobalt-60 Radiation Facility in Giessen

The radiation facility at the Justus-Liebig University Strahlenzentrum consist of a set of five powerful ^{60}Co sources with different activity. This mix allows for a wide range of different dose rates. By a slide valve the test object can be transported close to the sources leading to a dose rate $\approx 4\,\mathrm{Gy/min}$. This option is limited to small samples, it is used for all the quality control measurements of the PWO crystals. Another option is to lower the sources into the radiation room to setup complex experiments. Usually only the strongest of the five sources is used supplying a dose rate of $\approx 8\,\mathrm{Gy/h}$ at 1m distance. For some of the experiments we used one of the less active sources to reach radiation levels down to $10\,\mathrm{mGy/h}$ adapting closer to the conditions at $\overline{\mathrm{P}}$ANDA.

2.2 Experimental Program

Owing to the fact radiation recovery is a thermodynamical process, temperature imposes a strong impact on the timescales and appearance of recovery in PWO.
For any application of stimulated recovery in the experimental environment of $\overline{\mathrm{P}}$ANDA it is necessary to investigate the behaviour at a temperature of T=$-25\,$°C. To study the wavelength dependence of recovery light emitting diodes (LED) with different colors were used as external light sources.

2.2.1 The Experimental Setup

The experiment aims to quantify the radiation damage and recovery of the crystal by measuring the response to the γ-rays of a ^{60}Co γ-source $(1.17 MeV, 1.32 MeV)$ placed

PWO ID	TYPE	$\Delta k/m^{-1}$ @ 420 nm	wavelength /nm
960	1L	0,71	470
958	1L	0,72	510
1070	1L	0,72	525
1009	1L	0,71	640
962	1L	0,72	935
888	1L	0,41	1060
1007	1L	0,69	1060
861	1L	1,0	1060
1005	1L	0,71	1300
986	1L	0,71	1550

Table 2.1: Δk specifications of the 10 crystals along with the wavelength of the attached LED.

in front of the crystal.

The setup consists of 10 full size crystals of the shape 1L type in the barrel of $\overline{\text{P}}$ANDA. Eight of the crystals are chosen based on the radiation hardness in the range of $\Delta \text{k} = 0,7\,\text{m}^{-1}$ as shown in table 2.1. Two crystal have a lower and a higher radiation hardness to investigate the influence of the intrinsic properties to the stimulated recovery. Eight different wavelengths between $470nm$ and $1500nm$ have been chosen. Three crystal were equipped with an LED of an emission wavelength of $1060nm$. The crystals have been annealed before at $300\,°\text{C}$ for eight hours.

All of these are wrapped in multiple layers of teflon foil with an outer layer of aluminum and integrated into detector modules with Phillips/Photonis photomultipliers (XP1911) and 4 LEDs as lightsources. Each module contains 3 LEDs of identical wavelength and an additional blue LED as shown in Figure 2.1. Blue light showed the strongest impact on recovery at room temperature and can be used to recover the crystals faster in between different runs. Each LED can be switched individually, allowing to illuminate with one, two or three LEDs respectively. To couple the PMTs to the crystal a thin film of Baysilon silicone oil is applied before the modules are wrapped in black plastic for shielding light and added stability. The finished and tested modules are mounted on a copper cooling plate and placed inside a box made out of Styrodur with a thermal conductivity of $0,33\,\text{WK}^{-1}\text{m}^{-1}$ providing very good insulation. (Fig.2.3) Two temperature sensors (Pt100) have been placed inside of the box, one on the cooling plate the other one attached to a crystal side opposite to the cooling plate. Ensuring temperature stability throughout the experiment is crucial for the comparability of different measurements. The cooling liquid of choice is a mixture of 60% ethanol and 40% water. The cooling machine is a Huber CC-505 able to cool down to $-50\,°\text{C}$. For this setup it is very important that the cooling machine
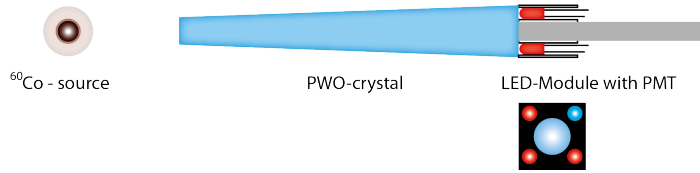
Figure 2.1: Side view drawing of one detector module including a front view of the LED/PMT part.
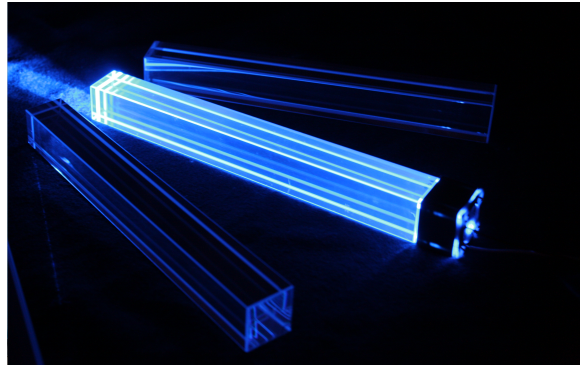
Figure 2.2: Working LED module with unwrapped crystal.

has enough headroom to compensate for temperature drifts during day- and nightime even in the summer month. This setup has been placed in the irradiation room at the Strahlenzentrum to be irradiated with the strong ^{60}Co sources. The PMTs and high voltage dividers where shielded with lead during the irradiation. During irradiation the PMTs were switched off. A dosimeter was used to determine the integral dose and the dose rate.

2.2.2 Measuring Program

After cooling the modules down to stable T$= -25\,°$C the response of a small ^{60}Co γ-source is measured. This is considered to be the reference value for the non irradiated crystal. Afterwards the irradiation is started with a dose rate of $8\,$Gy/h for 3h 45m to apply an integral dose of 30 Gy. Afterwards the detectors are measured again to determine the impact of the radiation damage. Immediately afterwards several recovery cycles are performed by illumination with light and measuring of the detector response. (Fig.2.5) The high voltage of the PMTs is switched off during illumination. This is done several times with an increasing illumination period starting from 5 minutes to several hours. To improve the results it is important to wait between measuring and illumination. The noise level of the PMTs has to stabilize after being illuminated. For the first run only one LED was used, the second run was undertaken
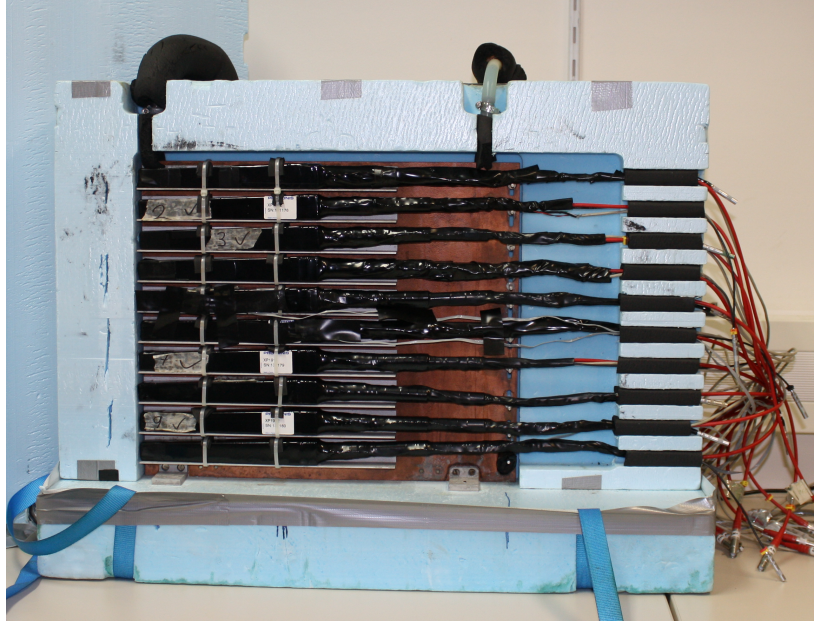
Figure 2.3: The finished setup, 10 PWO detector modules fitted on the copper cooling plate inside the isolation box.

with 2 LEDs. In between these two runs the crystals were illuminated with one blue LED and heated up to room temperature for more than 24 hours trying to recover as much radiation damage as possible without annealing the crystal in the oven at high temperature.

2.2.3 Analysis of the wavelength dependency

The analysis of the data is done using the software programs ROOT and Origin. The peak positions are determined by fitting an exponential decay function combined with a Gaussian as shown in 2.6

$$y = P1 + P3 \cdot e^{-\frac{x}{P6}} + \frac{P2}{P2 \cdot \sqrt{\frac{\pi}{2}}} \cdot e^{\frac{-2(x-P5)^2}{P4}} \tag{2.1}$$

where *P1* is the offset, *P2* is the area of the Gaussian, *P3* is the amplitude of the exponential, *P4* is the Gaussian width, *P5* the peak of the Gaussian and *P6* the decay constant of the exponential.

When all the peak positions are fitted these positions are compared relative to the value obtained before irradiation. The recovery of the light loss is then presented as a function of the integral time of illumination.
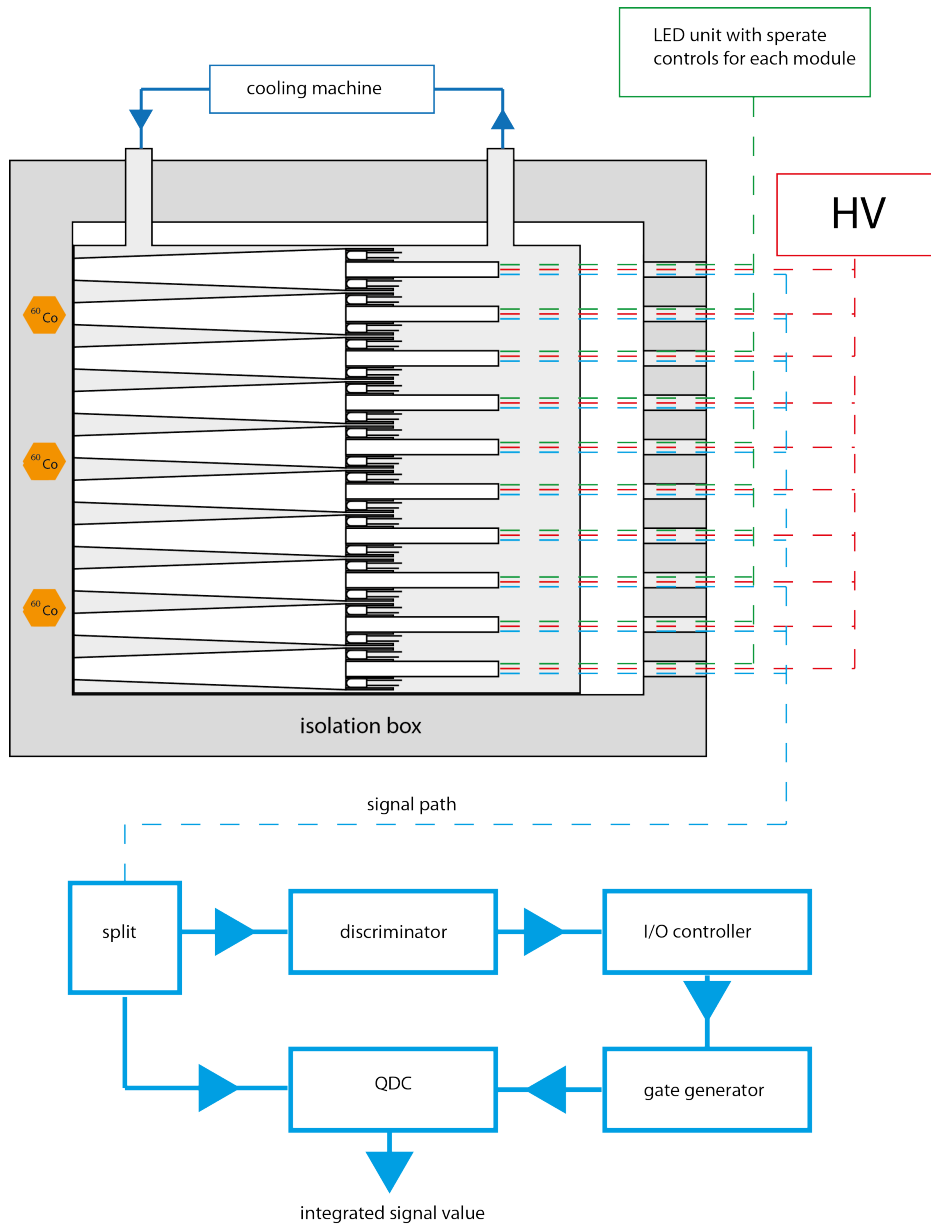
Figure 2.4: Schematical drawing of the 10-crystal setup with the readout electronic chain.

2.2.4 Analysis of Dependency of Wavelength and Photon Flux

From the obtained results it can be clearly deduced that the stimulation with light leads even in the cooled environment for wavelength up to $935nm$ to substantial recovery. However, the timescales become significantly longer compared to room tem-
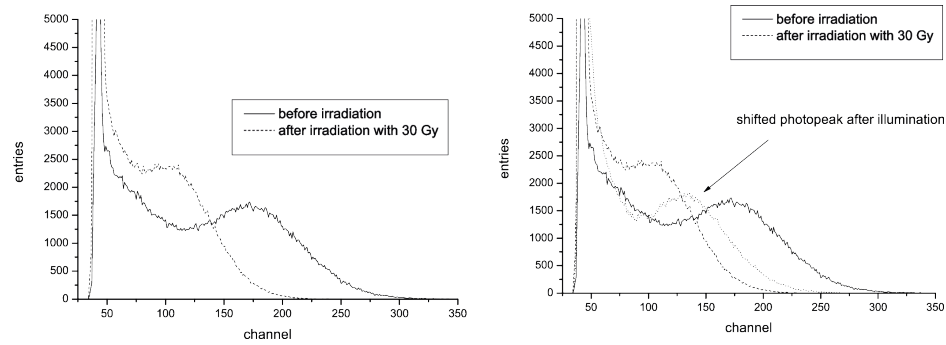
Figure 2.5: Left: Shift of the $1,33\,\mathrm{MeV}$ peak due to the irradiation; Right: Recovering due to illumination .
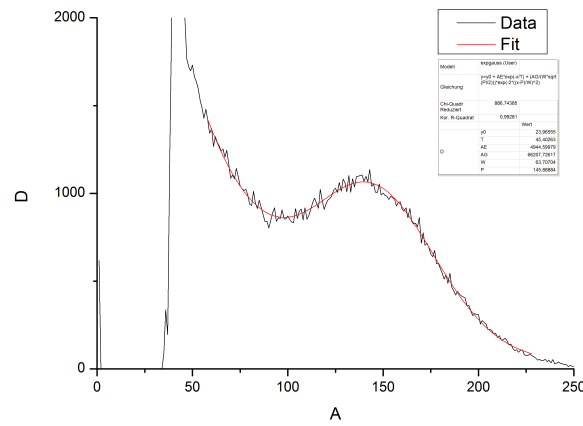
Figure 2.6: Fit of data to determine peak position.

perature but by far shorter than spontaneous relaxation.

The impact of the wavelength is similar to the behavior at room temperature. However, the maximum wavelength of a noticeable effect is shifted to values between $900nm$ and $1000nm$. The small effect at 1060 nm can be probably addressed to the width of the wavelength distribution of the LEDs with a tail towards the region below the limit. For the long wavelengths of 1300nm, 1500nm (Figures 2.9, 2.12) no effect has been observed. All the LEDs had the same photon flux in the order of 10^{16} photons per second. For the shorter wavelength no significant difference in the timescales becomes visible even when using more than one LED. In case of 1060 nm the flux of one LED leads to no recovery.At least two LEDs are necessary to indicate some slight recovery. The data shows that stimulated recovery appears more sensitive in the case of less radiation hard crystals as shown in Fig. 2.11. This could be explained by taking into account, that those crystals contain more defects and the stimulation might have a higher probability for initiating an effect.
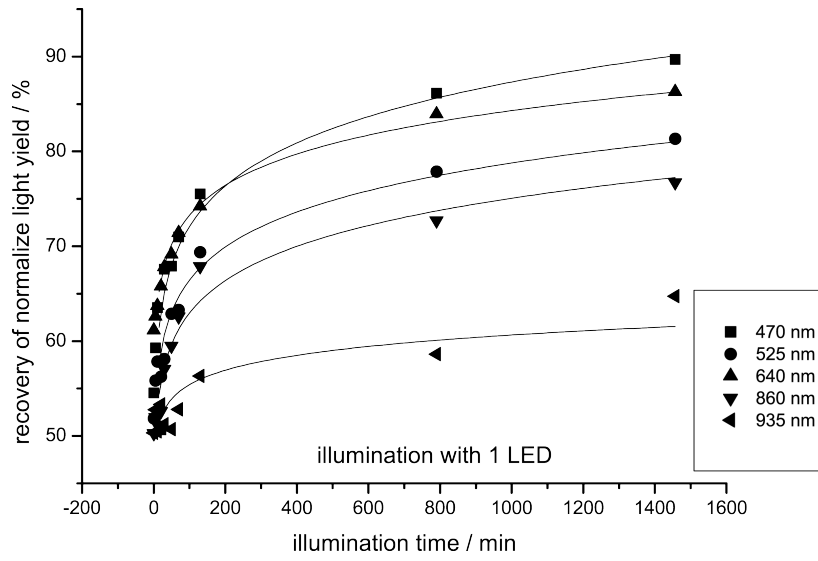
Figure 2.7: Recovery of the normalized signal amplitude as a function of the integral illumination time using a single LED with different short wavelengths.
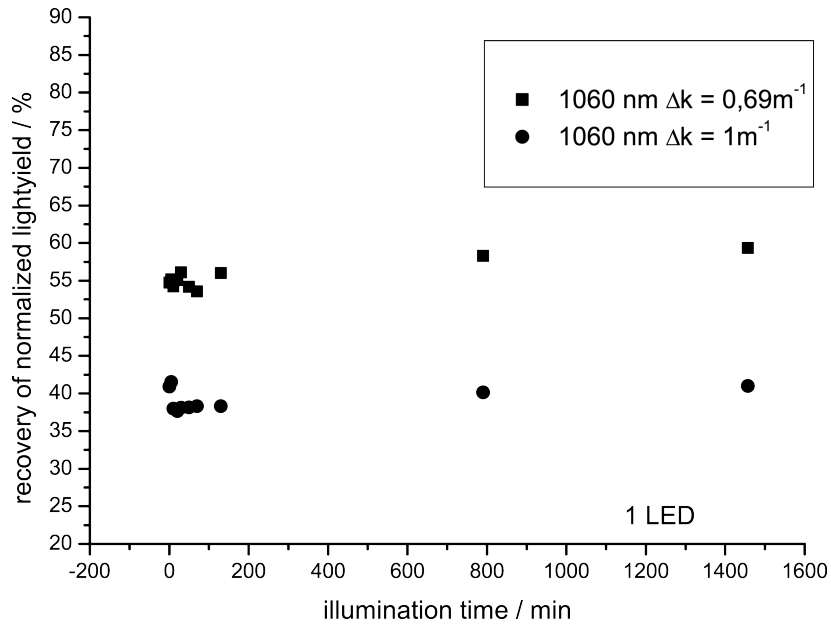
Figure 2.8: Recovery of the normalized signal amplitude as a function of the integral illumination time for a single LED with 1060nm wavelength for different Δk.
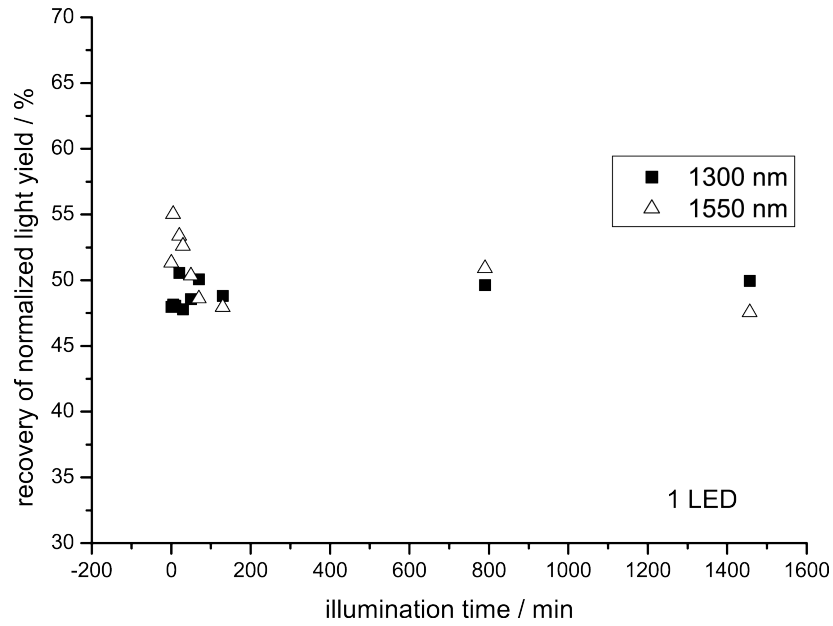
Figure 2.9: Recovery of the normalized signal amplitude as a function of the integral illumination time for a single LED with different long wavelengths.
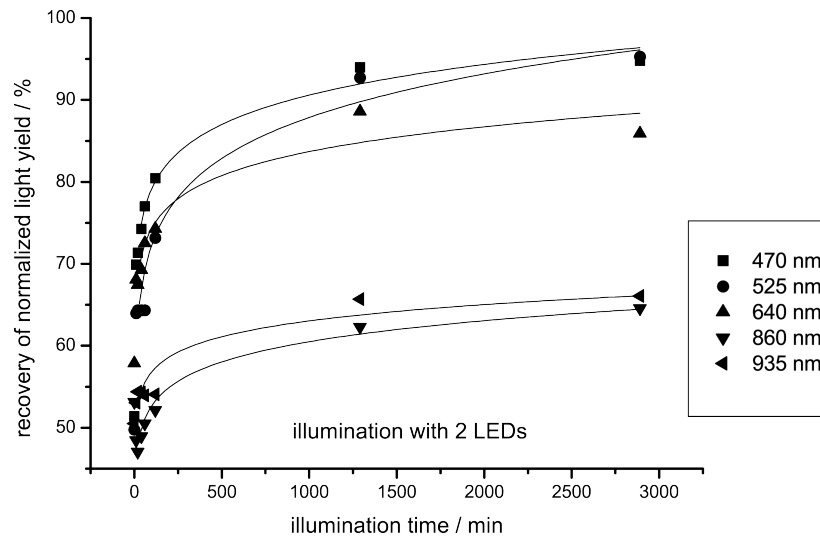
Figure 2.10: Recovery of the normalized signal amplitude as a function of the integral illumination time using two LEDs with different short wavelengths.
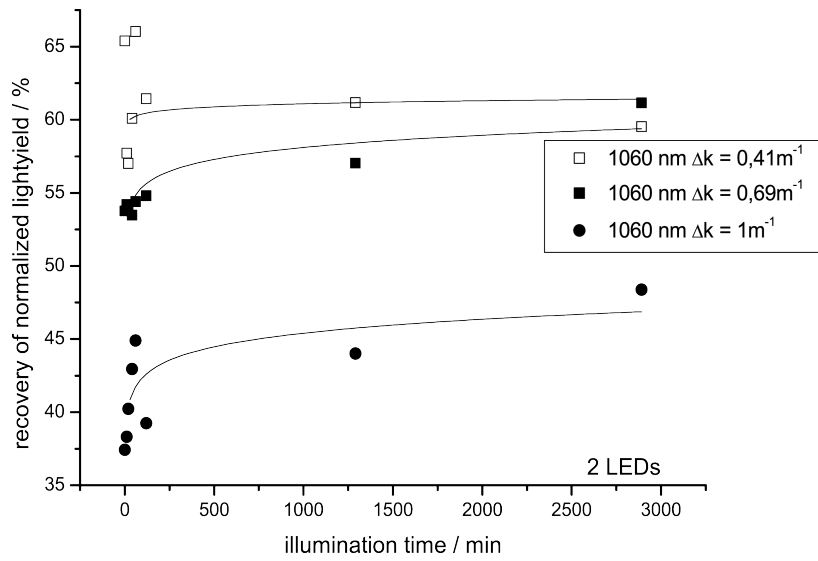
Figure 2.11: Recovery of the normalized signal amplitude as a function of the integral illumination time using two LEDs with 1060nm wavelength for different Δk.
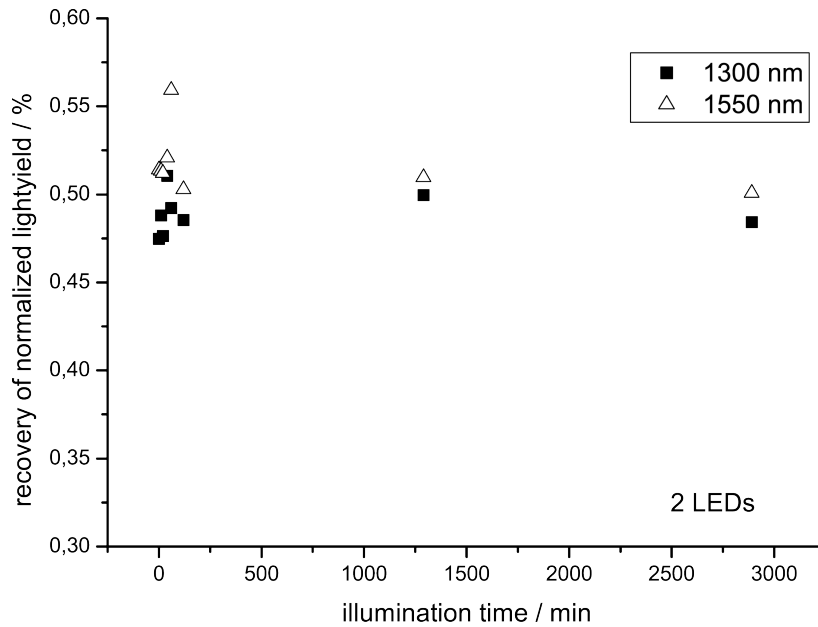
Figure 2.12: Recovery of the normalized signal amplitude as a function of the integral illumination time using two LEDs with different long wavelengths.

Chapter 3

Online Recovery

Online recovery considers the application of stimulated recovery parallel to the irradiation of the crystals. As discussed in the introduction the idea of in situ recovery would allow for more stable beamtime conditions resulting in higher efficiency and longer runtimes.

3.1 First Steps

3.1.1 Proof of Concept

A first pilot experiment has delivered positive results. Four detector modules were assembled in a similar way as described in Chapter 2. The used wavelengths were 460, 525, 630, 935nm, respectively. Each crystal module was equipped with four LEDs of the same kind, with a total photon flux between 10^{16} and 10^{17} photons per second. The crystals were cooled down to T$=-25°C$ and then irradiated for 4 hours with a dose rate of $0.1Gy/h$ but illuminated by the LEDs in parallel. Before and after the irradiation/illumination process the response to γ-radiation from a ^{60}Co-source was measured. Figure 3.1 shows the overlay of the response spectra before and after irradiation. Slight shifts of the photo peak stay below 10%, well below an expected light loss of nearly 50%

3.1.2 Quantifying the Online Recovery Process

In a next experiment the dose rate was significantly reduced towards a value more closer to the final experimental conditions at $\overline{P}$ANDA. The same 10-crystal setup which was also used in the former experiment (see Chapter 2.) was placed at a larger distance to the ^{60}Co-source adjusting a dose rate of $10mGy/h$. The integral dose was controlled by a dosimeter placed next to the experiment. The ten crystals were
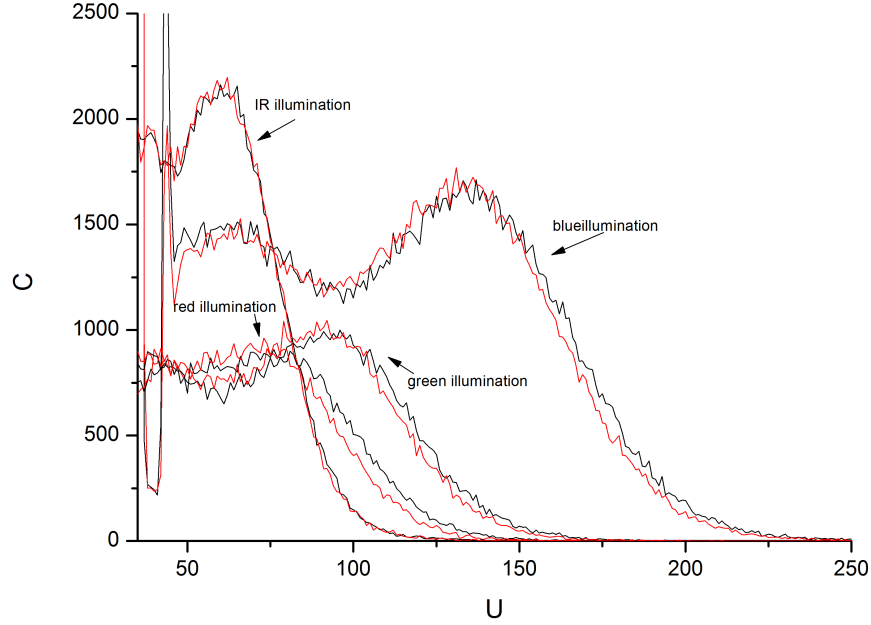
Figure 3.1: Response of PWO to a low energy photons of a ^{60}Co-source measured before(black) and after(red) irradiation with $30Gy$ and in situ illumination of each crystal with 4 high power LEDs.

illuminated online with only one LED and a flux in the order of $10^{15} \leq 10^{16}$ photons per second. For technical reasons the test were performed at a temperature of T=$-20,3°C$. Two runs were performed, one with illumination and one without. The illumination run was done first and the crystals were irradiated with $10mGy/h$ for 12 hours. Again the response to a ^{60}Co-source placed directly in front of the crystals was measured before and after irradiation. The photon peak was then fitted and the two measurements compared relatively to each other. Afterwards the blue LED in each detector module was switched on for 12h to recover any remaining damage to prepare the next experiment without thermal annealing. The second run was conducted without illuminating. The results are summarized in Figure 3.2. However, the results are not conclusive due to missing sensitivity. The small effect of the radiation damage is comparable to the experimental uncertainty of determining the position of the photo peak.

Figure 3.2: Recovery of normalized light yield for different wavelength at low irradiation dose of $10mGy/h$.

3.2 Online Recovery with 2"-PMTs

3.2.1 Experimental Setup

To address the above issues a new setup has was prepared. The use of Hamamatsu R2059-001 SEL Bialkali photomultiplier tubes with 2" diameter ensured that the full end surface of the crystal is covered and all scintillation photons can be converted. A coupling module has been fabricated to connect the PMT and the crystal, as well as hold the LEDs. The next major difference to the setups used before is the position of the LED. In the other setups these were located next to the PMT on the rear face of the crystal to allow for maximum efficiency of the light coupling. Here it is not possible due to the size of the PMT. The LED is positioned on the upper side of the crystal at an angle of 45° with respect to the surface. The crystal is wrapped in teflon and aluminum foil but a small entrance window has been opened for the light. For better optical coupling between the crystal and the PMT a thin layer of Baysilon silicone oil is applied. The detector modules are again mounted on a copper cooling plate. One temperature sensor (Pt100) is attached to the copper plate and another one to one of the crystals. The insulation box is again composed from Styrodur with 10 cm thickness. To further address the temperature stability of the whole system the

PMTs are now located in the outer walls of the box and the HV divider is completely on the outside. This minimizes the heat dissipating into the box.

PWO-crystal   LED-Module with 2″-PMT
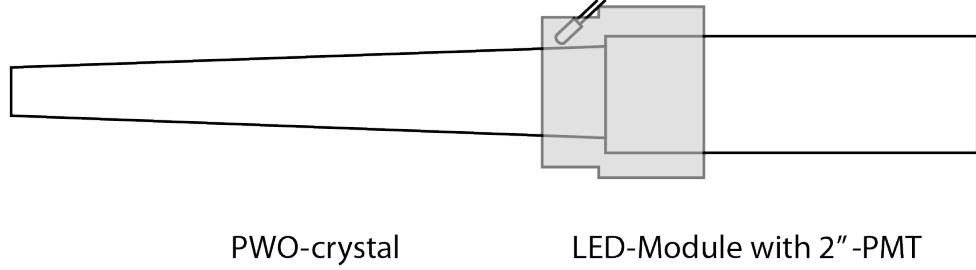
Figure 3.3: Schematical drawing of the new coupling to illustrate the led position.
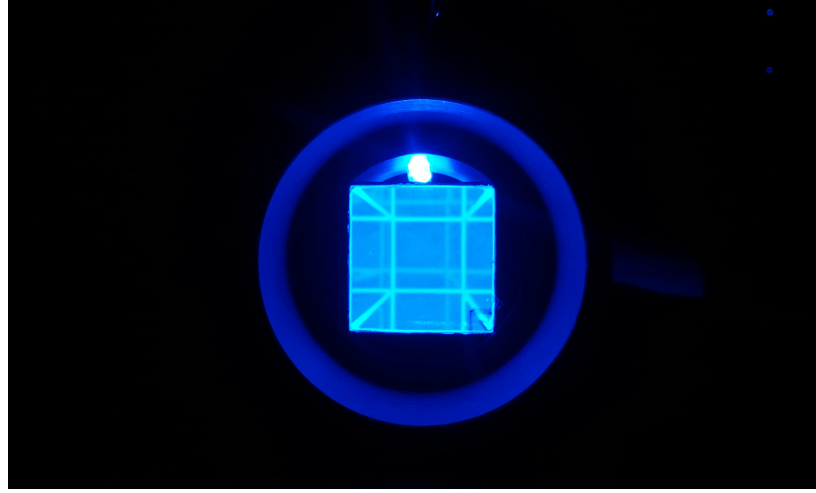
Figure 3.4: View inside the crystal module from the PMT point.

A ^{60}Co-source is placed in front of the crystals. A different ^{60}Co-source with an activity of $91.06GBq$ was chosen to supply a dose rate similar to $\overline{P}$ANDA beamtimes. The experiment was placed at a distance of 1.85 m from the source and the PMTs were shielded by a lead wall.

Two runs were performed: one low flux illumination run with a photon flux of $10^{14}ph/s$ and one high flux run with $10^{16}ph/s$, calibrated by a precise controlling of the LED current. The total flux of the LEDs was calibrated with an Ulbricht sphere and a spectrometer before. After cooling for more than 24h to achieve thermal stability, the irradiation was started with the low flux illumination. The dose rate was recorded with a dosimeter. The rate used was $10mGy/h$ and it was irradiated for 130h until a integral dose of $1.3Gy$. Throughout the run the temperature was kept at T=$-25°C$ with a maximal deviation of $0.5°C$. One measurement was taken before and one after irradiation. Assuming the radiation damage has not reached saturation level the

Figure 3.5: The completed setup alongside the Huber cooling machine.

crystals were irradiated again with the same dose to have a damage reference without illumination. Afterwards the setup was heated to room temperature and left for 24h to recover slightly before being cooled down again to prepare for the high flux run. The irradiation time for the high flux run was slightly longer with an accumulated dose $1.5Gy$. Again two measurements were taken before and after irradiation with illumination. A third measurement was made after irradiating the crystal again with $1.5Gy$ without illumination.

3.2.2 Results

The peak positions, determined as shown in Chapter 2., were compared to each other. The damage is quantified as a loss of the normalized signal amplitude with respect to the value before irradiation. The results can be seen in Table 3.1. The long irradiation time and the bigger PMTs allowed for a much better quantification of the effect. Whith the better sensitivity and longer irradiation times it can be deduced from the obtained results that in situ illumination has a strong effect on the sgnal response. Keeping the signal loss rates lower, when compared to non illuminated irradiation. Online recovery is quite efficient for short wavelengths, even at T= $-25°C$. The amount of recovery is also highly photon flux dependent for a given dose rate. When a specific saturation level is reached even more damage is recovered than is newly formed. The higher than 100% values for the high flux run appear due to the previous damage imposed onto the crystal with the first irradiation cycle. However, the results show no recovery for an

wavelength	Low Flux Mode 10^{14} photons/s normalized signal response /%			High Flux Mode 10^{16} photons/s normalized signal response /%	
	online recovery	no illumination		online recovery	no illumination
470nm	98.9	70.7	89.8	116.2	67.7
525nm	87.7	77.9	89.8	109.5	77.3
670nm	88.5	78.7	87.0	106.3	78.2
935nm	81.2	84.2	87.7	88.5	84.9

Table 3.1: Normalized signal response after irradiation with respect to the starting value and in situ illumination of the crystals, the middle column shows the signal response after some recovery period between the low flux run and the high flux run with respect to the absolute starting value.

illumination wavelength of 935nm at low temperatures. The previous observed small amount of recovery in this region probably stems from the fact that the wavelength distribution of the LED is more than 50nm wide. Combined with a much higher flux this could provide enough photons below the cutoff to achieve stimulated recovery.

Chapter 4

Electron Paramagnetic Resonance

Electron Paramagnetic Resonance (EPR) is a spectroscopic technique depending on the permanent magnetic moment of unpaired electrons. Relying on the microwave absorption of a sample in an outer magnetic field it offers a qualitative analysis of the electron structure inside the crystal.

When a sample with a permanent magnetic moment is exposed to an external magnetic field the degeneracy is broken and the energy levels split up. This is called the Zeeman effect, the split up exists because of different interactions between the magnetic field and the electrons with different quantum numbers due to the different orientation of the related magnetic moment with respect to the quantization axis. In case of a free unpaired electron two different energy levels result as seen in Figure 4.1. The elec-
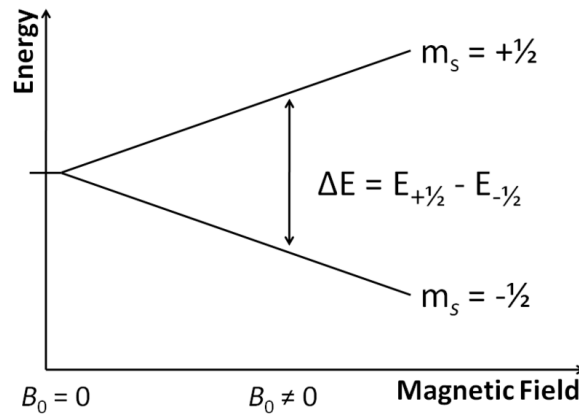
Figure 4.1: Diagram showing the energy level splitting due to the Zeeman effect of electron spin moments in an applied magnetic field with strength B_0. [Wik11]

trons with different spin orientations are distributed among the corresponding energy levels according to the Boltzman statistics (since they represent isolated, independent systems) and can perform transitions between the lower and upper state by either absorbing or emitting electromagnetic radiation matching ΔE if the condition

$$h \cdot \nu = g \cdot \mu_B \cdot B \qquad (4.1)$$

is fulfilled. In most cases microwaves are used to excite the electrons which requires magnetic fields of some tenth of a Tesla (e.g. appr. $300mT$ at $10GHz$). One can either vary the frequency of the microwaves to match ΔE or the magnetic field strength thus widening the energy gap until it matches the used microwave energy. Normally the frequency is kept fixed and the magnetic field is varied and the absorption of microwaves is monitored to find the resonances which show up in the experiment as a net absorption due to the higher occupancy of the lower energy state (this of course depending strongly on temperature). Electrons in a solid state may experience, in addition to the external field, crystalline electric fields with definite symmetries and local magnetic fields due to the nuclear magnetic moments of the own or neighboring nuclei. This causes further splitting of the energy levels which in addition may depend on the orientation of the crystalline axes with respect to the external magnetic field. This results in more complicated, angular dependent EPR spectra with sometimes rich structure, but on the other hand provides detailed information about the microscopic structure of the paramagnetic center under investigation.

4.1 Experimental Setup and Procedure

A small brass cooling module was built to perform this experiment, the unit consists of 5 light tight chambers with the crystal in the center and LEDs with different wavelength right above. Figure 4.2 shows a cut through one chamber. The crystal shards were already attached to the holding structure for the EPR measurement to ensure easy handling after irradiation (Figure 4.3). The whole setup was again placed into a custom build Styrodur box to further insulate the setup against the outside temperature.
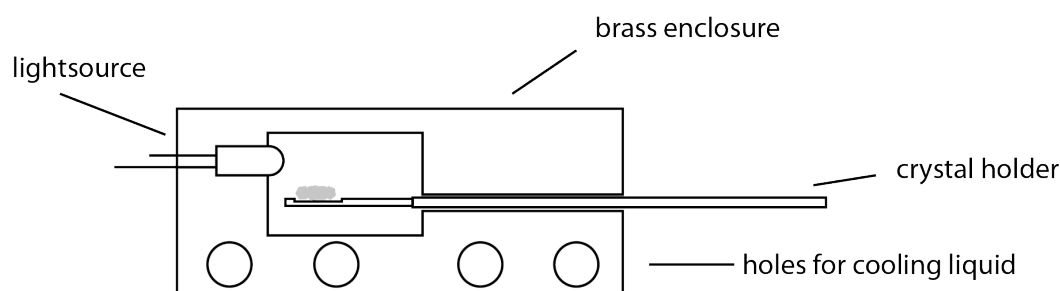
Figure 4.2: Cut through one of the five illumination chambers inside the cooling module.

Before and while cooling the setup was flooded with gaseous nitrogen and kept under overpressure to prevent ice formation in the chambers. After everything was cooled

Figure 4.3: Closeup of one crystal sample already attached to the EPR holder.

down to T $= -25°C$ the crystals were irradiated with the ^{60}Co source at the Strahlen-zentrum for 30 minutes at an average dose rate of $8Gy/h$. After the irradiation was done the crystals were illuminated for 30 min with wavelengths of 425 nm, 525 nm, 640 nm and 1060 nm. One sample was not illuminated and kept dark to have a reference without recovery. After being taken out of the enclosure the crystals were placed in liquid nitrogen and kept in total darkness to exclude any further recovery processes. The measurements were performed in the 1. Physical Institute of Justus-Liebig Universität.

4.2 Results and Analysis of the EPR Measurements

As expected a illumination wavelength dependent effect can be seen in these measurements. Consistent with the light yield recovery test, shorter wavelength lead to a greater change. In Figure 4.4 the growing center has been clearly identified as $(MoO_4)^{3-}$ by its (angular dependent) g factor and the hyperfine structure. The different resonance positions are due to different orientation of the sample in the field. Furthermore the not illuminated crystal shows that this response is clearly induced by the photons shifting the electrons from more stable centers towards this deeper trap. The infrared illuminated crystal shows the cutoff effect earlier observed in all the other tests. Figures 4.5 and 4.6 show again the $(MoO_4)^{3-}$ center. The first one giving a qualitative overview of the EPR spectra, while the latter one shows their intensity normalized to the maximum value of the 425 nm illuminated crystal.

What is shown here is in good agreement with the stimulated recovery test and the online recovery test. It even provides an answer where the other tests only give a quantitative view of the recovery.
The stimulated recovery via illumination is due to an emptying process of deep traps
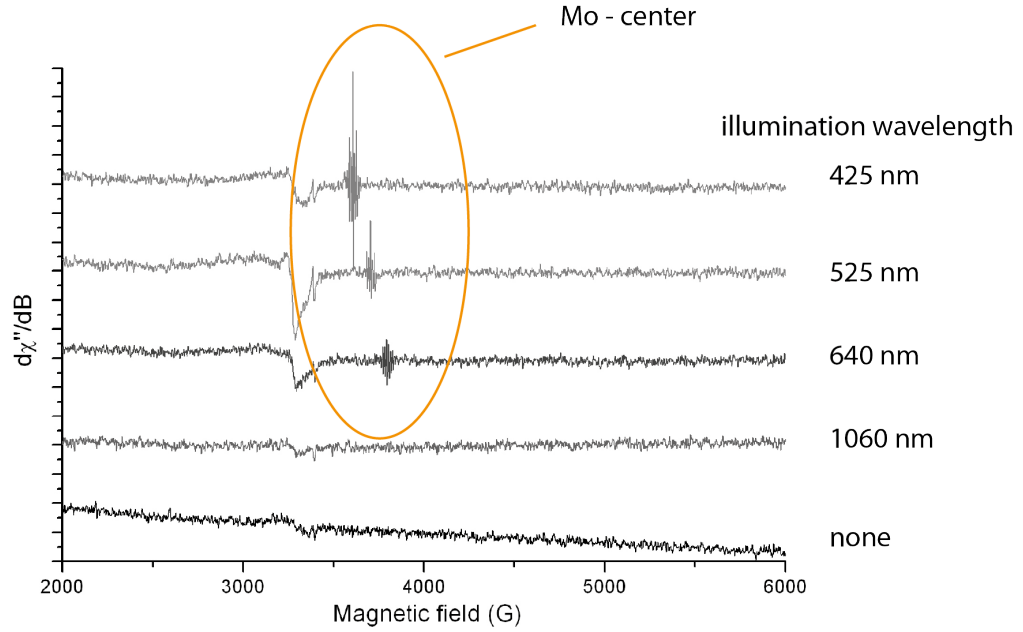
Figure 4.4: EPR spectra for the four different wavelength showing the rise of the $(MoO_4)^{3-}$ center.
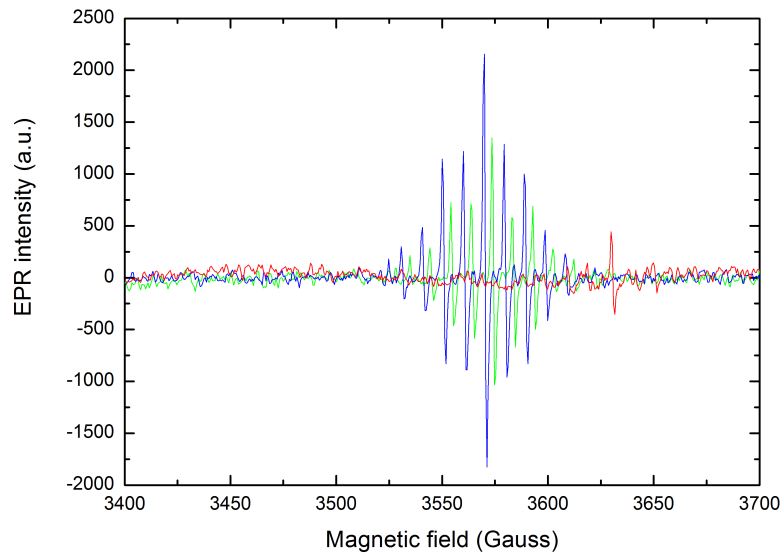
Figure 4.5: The EPR intensity of the $(MoO_4)^{3-}$ center for different illumination wavelength (blue 425nm; green 525nm; red 640nm.)
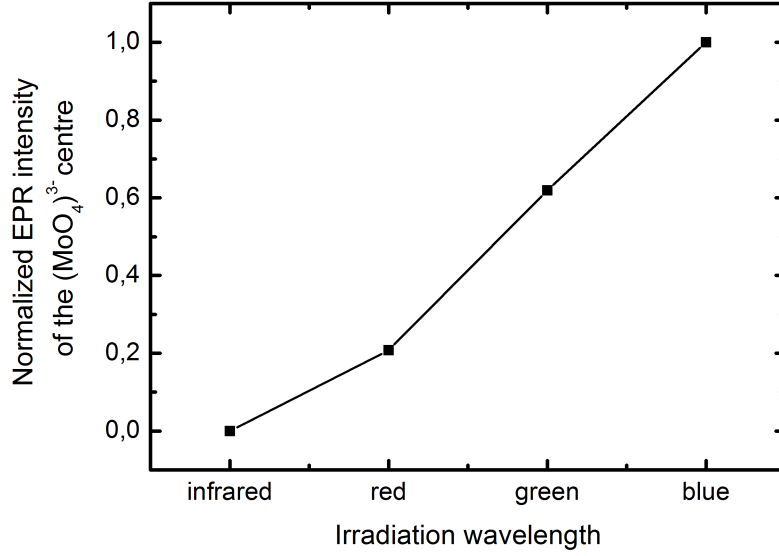
Figure 4.6: The normalized EPR intensity of the $(MoO_4)^{3-}$ center for different illumination wavelength (blue 425nm; green 525nm; red 640nm; infrared 1060nm.)

with an activation energy to large to be overcome by thermal activation at T=$-25°C$ (appr. $25meV$). The fact that light of 1060 nm ($\approx 0.8eV$ optical energy) provides another measure of this trap depth. With higher energy (lower wavelength) the trapped electrons then can be more and more transferred into the conduction band where they are mobile until they are trapped at $(MoO_4)^{2-}$ complexes. Since the $(MoO_4)^{3-}$ trap is metastable at T=$-25°C$ (in contrast to room temperature, where it has very short lifetime) it catches the electrons effectively and thereby prevents them from further contribution to the absorption band disturbing the scintillation light yield. They should, however create a new absorption near 530 nm which after all does not spoil the detector performance. A direct proof that such an absorption arises is still missing due to experimental problems.

With respect to the nature of the center responsible for the hazardous part of the absorption only a first indication exists until now. Parallel to the rising of the $(MoO_4)^{3-}$ the EPR spectrum of a paramagnetic center dissapears whose resonance position and structure shows some similarity to the $Pb^+ - V_O$ center described in literature. More detailed measurements and by that a quantitative analysis, however, haven't been possible until now because of experimental difficulties.

Chapter 5

Conclusion and Outlook

The operation of inorganic crystalline scintillation materials for detector applications in an environment of strong irradiation requires resistivity to the damage due to ionizing radiation. For electromagnetic calorimetry in high-luminosity hadron accelerator experiments this problem becomes crucial.

In the case PWO-II as scintillator the radiation damage consists purely of the creation of different color centers with a combined wide absorption band. This shortening of the light attenuation length substantially impacts the signal response of the detectors by self absorption of the scintillation photons. For parts of the $\overline{P}$ANDA-EMC, with a proposed maximum radiation dose of $30Gy$ in the most forward region, this results in a transmission loss of $\approx 40\% - 50\%$. It is important to find methods to counteract this damaging process to ensure stability and long runtimes. Under normal conditions the spontaneous relaxation of the color centers, given enough time, allows for total recovery of damage imposed by γ-radiation. However spontaneous relaxation is a thermo-activated process which is only fast at high temperatures and the operation temperature of the $\overline{P}$ANDA-EMC is $-25°C$ rendering its effect negligible. [ea07] Additionally to the temperature, the relaxation process can be influenced by a higher flux of energy interacting with the color centers. One process would be optical bleaching by the use of UV light, this requires much higher energies than thermo activation would due to inefficiency in the ionization process. Another process which is called stimulated recovery, relying on an intra center resonant transition, works even for infrared light. Up to now this process has only been shown to deliver impressive results at room temperature, to be applicable to the $\overline{P}$ANDA experiment it is required to operate at T=$-25°C$.

5.1 Achieved Results

The experiments described in this thesis have proven that stimulated recovery is working even at T=$-25°C$. Not as powerful as at room temperature, the obtained results
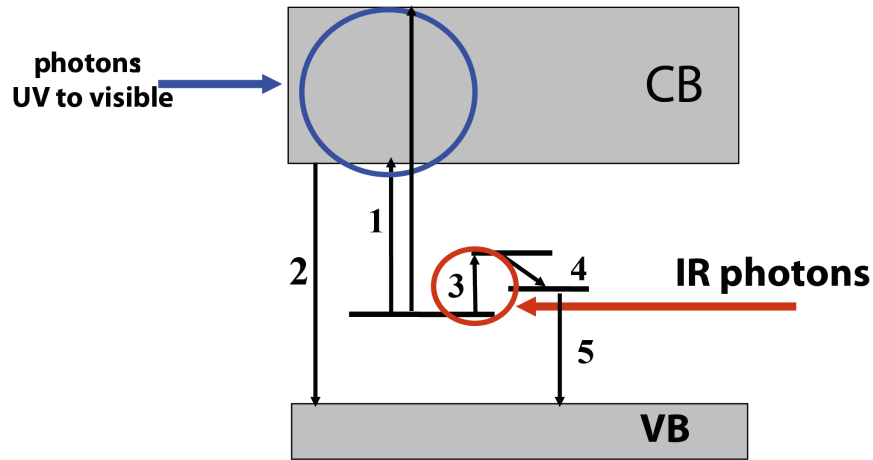
1 ionization of FTD_0,   **2** radiative/nonradiative recombination,
3 intra-center absorption in FTD_0,   **4** non-radiative relaxation,
5 radiative/nonradiative recombination of FTD_0.

Figure 5.1: Proposed relaxation scheme for stimulated recovery at room temperature.[Nov10]

remain impressive. The first striking difference is the longer timescale of recovery when comparing to room temperature. For example, when illuminating with blue light the recovered amount of light yield loss in a given time frame is ≈ 10 times lower at $-25°C$. Total recovery was never observed in the measured timescales. These two observations can possibly be attributed to the freeze out of spontaneous recovery in cold crystals. In a warmer regime the process of stimulated recovery and spontaneous relaxation coexist, which will ultimately lead to 100% recovery, as can be observed with very long timescales for spontaneous recovery alone. Another point to address is the difference in wavelength dependency. From the results we can state that there is a definite cutoff between 900nm and 1000nm. Above this limit the recovery process can not be speed up by stimulation with light. The difference of 45K in temperature resulting in the reduction of lattice vibrations and the stokes shift of the transitions could be responsible. It can be stated that there is a definite correlation between photon flux and the amount of recovery, probably stemming from the higher crossection and the higher integral energy. However it can be seen that this correlation is also influenced by the amount of colour centers. Further research is needed to determine the optimum settings wavelength and photon flux with respect to the dose rate. Online recovery has been achieved with impressive results for short wavelengths. With the appropriate amount of illumination the performance of the detector modules could be
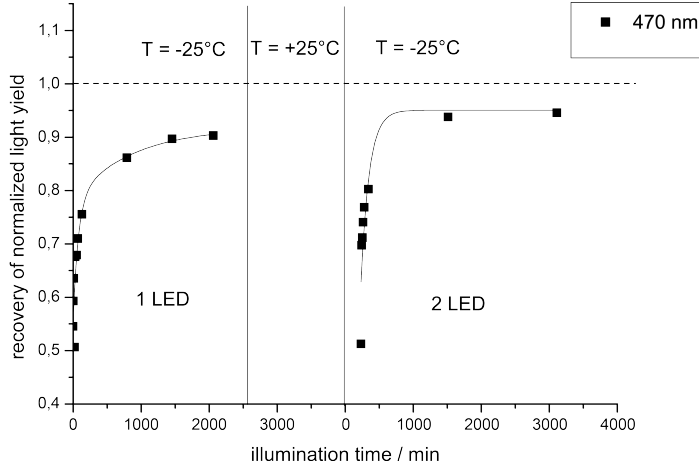
Figure 5.2: Difference between a induced photon flux of $\approx 10^{16}$(left) and $\approx 10^{17}$(right) for a crystal irradiated with $30Gy$ at T$=-25°C$.

operated in stable mode. If the used sensors are blind for the illumination source this would be a perfect solution. For the $\overline{\mathrm{P}}$ANDA-EMC two different scenarios exist. The barrel will be equipped with APDs and the endcaps with vacuum phototriodes both with a totally different quantum efficiency. As shown in Fig.**??** for the barrel APDs online recovery won't be possible considering that stimulated recovery does not work in the far infrared region for cooled crystals. On the other hand, the endcaps with a much higher radiation exposure are blind in the red- near-infrared region, where recovery still can be accelerated. For the barrel the application of offline recovery in between beam periods would drastically shorten the downtime of the experiment. It could even be applied when the EMC is still kept cool.

Addressing the mechanism of stimulated recovery, EPR measurements delivered first results. It has been shown that $(MoO_4)^{3-}$-trap will rise with the recovered light yield, effectively retrapping all electrons brought into the conduction band. This trap does not interfere with the main luminescence signal, due to a different absorption wavelength. Further can be deduced from the EPR measurements that the recovered trap depth is somewhere between $700meV$ and $800meV$ which hints towards a known Frenkel type defect. But these measurements are only a first indication to what kind of defect is responsible for the crucial part of absorption. More tests have to be done in this regard.
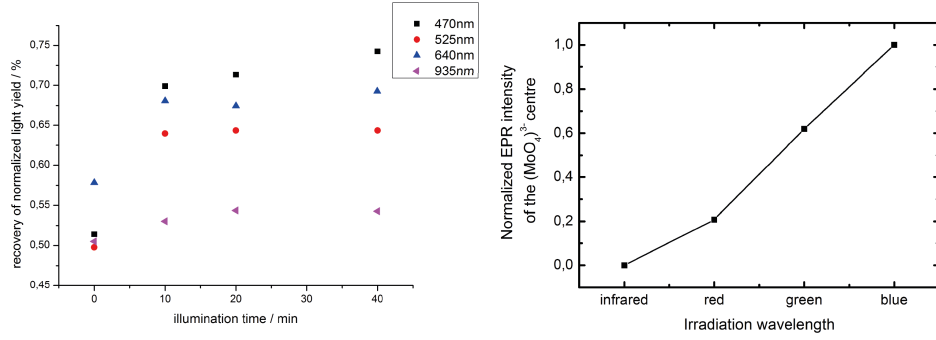
Figure 5.3: left: recovery of normalized light yield; right: qualitative signal strength of $(MoO_4)^{3-}$ after illumination.

5.2 Outlook

To acquire more knowledge about the traps and defects leading to the hazardous absorption in the first place, it is of great importance to have transmission measurements at T$=-25°C$. In order to achieve this, a new setup was built and tested which will be able to measure a cooled crystal before and after irradiation. The setup consists
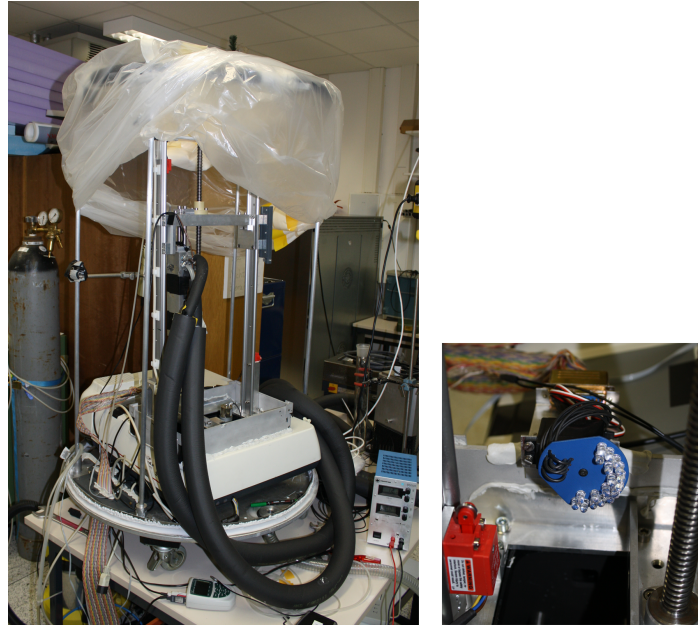
Figure 5.4: Left: Spectrometer with elevator. Right: LED illumination device

of a double beam spectrometer with an attached crystal elevator on top. This allows to place it inside of the radiation chamber and shielding the spectrometer, while ir-

radiating the crystal. Shown on the right side in Fig. 5.4 the newly built rotating LED device to observe the different changes of the transmission spectra with respect to various illumination wavelengths. The biggest problem is the formation of ice on the crystal surface, which is addressed by insulating the setup and flooding it with dry nitrogen keeping everything under pressure for the duration of the experiment.

The transmission measurement will, in combination with the EPR,allow for a qualitative analysis of the recovery process. Then one will be able to directly identify the centers which are affected by any given wavelength.

Regarding the technical application of the stimulated recovery mechanism within the $\overline{\text{P}}$ANDA-EMC, it can be suggested to implement an online recovery setup into the forward endcap, as it is most prone to radiation damage. For the barrel the only feasible implementation would be offline recovery, due to the used APDs.

List of Figures

Bibliography

[AKL02]   A.A. Annenkov, M.V. Korzhik, and P. Lecoq. Lead tungstate scintillation material. *Nuclear Instruments and Methods in Physics Research A 490*, 2002.

[Col08]   PANDA Collaboration. Technical design report for panda. 2008.

[Col09]   PANDA Collaboration. Physics performance report for panda. 2009.

[Dor]   Valera Dormenev.

[ea07]   P.A. Semenov et al. First study of radiation hardness of lead tungstate crystals at low temperatures. 2007.

[ea11]   K. Nakamura et al. *J. Phys. G 37, 075021 (2010) and 2011 partial update for the 2012 edition.* Particle Data Group, 2011.

[Hof10]   Albrecht Hofstaetter. Group lecture on pwo. 2010.

[Kit96]   Charles Kittel. *Introduction to Solid State Physics 7. Edition.* John Wiley and Sons, 1996.

[LAG+06] P. Lecoq, A. Annenkov, A. Gektin, M. Korzhik, and C. Pedrini. *Inorganic Scintillators for Detector Systems.* Springer Verlag, 2006.

[LDA+95] P. Lecoq, I. Dafinei, E. Auffray, M. Schneegans, and M. V. Korzhik et al. Lead tungstate (pbwo4) scintillators for lhc em calorimetry. *Nuclear Instruments and Methods in Physics Research Section A: Accelerators, Spectrometers, Detectors and Associated Equipment, November*, 1995.

[Met08]   Volker Metag. Group lecture, 2008.

[Nov10]   Rainer Novotny. Radiation damage and recovery of pwo-ii crystals. Talk given towards the CMS Collaboration, 2010.

[PL06]   F. Nessi-Tedaldi F. Pauss P. Lecomte, D. Luckey. High-energy proton induced damage study of scintillation light output from pbwo4 calorimeter crystals. 2006.

Bibliography

[QD99]   Ren-yuan Zhu Qun Deng, Zhiwen Yin. Radiation-induced color centers in la-doped pbwo4 crystals. *Nuclear Instruments and Methods in Physics Research A 438*, 1999.

[Wik11]   Wikipedia. Electron paramagnetic resonance, 2011.

[WZAH99]   R. T. Williams, Y. C. Zhang, Y. Abraham, and N. A. W. Holzwarth. Electronic structure of pure and defective pbwo4, cawo4 and cdwo4. *SCINT Proceedings*, 1999.

[XDQC00]   L. Y. Zhang X. D. Qu and R. Y. Zhu (CMS Collaboration). Radiation induced color centers and light monitoring for lead tungstate crystals. *IEEE Trans. Nucl. Sci. 47*, 2000.

[yZ98]   Ren yuan Zhu. Radiation damage in scintillating crystals. *Nuclear Instruments and Methods in Physics Research A 413*, 1998.

Danksagung

Es wurde einmal gesagt, daß für jeden noch so großen Ozean ein Schiff gebaut wurde um es zu überqueren. So ein Schiff baut sich schlecht allein und so möchte ich diese Gelegenheit nutzen um mich bei denen zu bedanken, die mir geholfen haben dieses Schiff zu bauen.

An erster Stelle danke ich Prof. Volker Metag und Dr. Rainer Novotny für die Aufnahme in Ihre Arbeitsgruppe und die unermüdliche Unterstützung und das Vertrauen, dass sie in mich gesetzt haben bei all den verschiedenen Projekten. Es hat einige Jahre gedauert von der Detektorkonstruktion für TAPS in Bonn bis jetzt zum PANDA-EMC, aber es waren lehrreiche und freudige Jahre in dieser Arbeitsgruppe, eine Zeit die ich nicht missen möchte.

Auch dieser Arbeitsgruppe möchte ich danken, Menschen ohne die solche Arbeiten nicht möglich wären, ohne die man verzweifeln oder scheitern würde, ohne die keine Zeit zum Lachen wäre, ohne die man an Technik oder Bürokratie verzweifeln würde. Ganze besonders möchte ich Rene Schubert danken, der mir in allen technischen Belangen stets zu Seite stand und ein guter Freund geworden ist. Nicht zu vergessen sind auch Daniel, Markus und Tobias die das beste Büro der Welt bilden und auf fast jede meiner Fragen kompetente Antworten wissen. Valera für unermüdliche Hilfe und stetes Interesse. Nicht zu vergessen Henning und Karoly stets darauf bedacht auch die Welt jenseits der Physik nicht zu vergessen. Albrecht Hofstaetter und Jan Stehr danke ich für die unglaublich kompetente Unterstützung mit den ESR- Messungen.

Ganz besonderer Dank gilt Benjamin, Joschka, Michaela und Nico für das Lektorat und die Tatsache, dass sie mich mein ganzes Studium und länger als Freunde begleiten und mein Leben unglaublich bereichern.

Als nächstes möchte ich meiner Mutter Charlotte danken, dafür, dass sie einen immer unterstützt wenn man es braucht oder einem ins Gewissen redet, wenn es denn nötig ist. Die immer an einen glaubt, selbst wenn man selbst zweifelt. Nicht zu vergessen Simon und Maren, die wahrscheinlich beste Verwandtschaft, die man haben kann.

Einen extra Absatz widme ich Verena, dem Sonnenschein meines Lebens. Mich während dieser Diplomarbeit zu ertragen, dafür kann man sich kaum bedanken. Ich will es trotzdem versuchen. Danke!

Hiermit versichere ich, dass diese Arbeit ohne Hilfe Dritter und ohne Benutzung anderer als den angegebenen Quellen und Hilfsmittel angefertigt wurde.

Diese Arbeit wurde in gleicher oder ähnlicher Form noch keiner Prüfungsbehörde vorgelegt.

Till Kuske
Gießen, im September 2011